

RS2 THEORY

# **PM4SILT (VERSION 1): A SILT PLASTICITY MODEL FOR EARTHQUAKE ENGINEERING APPLICATIONS**

# Table of Contents

## PM4SILT (VERSION 1): A SILT PLASTICITY MODEL FOR EARTHQUAKE ENGINEERING

<b>APPLICATIONS .....</b>	<b>1</b>
<b>1- Introduction.....</b>	<b>3</b>
<b>2- Model Formulation.....</b>	<b>3</b>
2.1- Basic stress and strain terms.....	3
2.2- Critical state .....	4
2.3- Bounding, dilatancy, and critical surfaces .....	5
2.4- Yield surface and image back-stress ratio tensors.....	7
2.5- Stress reversal and initial back-stress ratio tensors .....	8
2.6- Elastic strains and moduli .....	9
2.7- Plastic components without fabric effects .....	10
Loading index.....	10
Hardening and the update of the back-stress ratio.....	11
Plastic modulus .....	12
Plastic volumetric strains - Dilation.....	12
Plastic volumetric strains - Contraction .....	14
2.8- Fabric effects .....	15
Additional memory of fabric formation history .....	15
Effect of fabric on plastic modulus.....	16
Effect of fabric on plastic volumetric dilation .....	17
Effect of fabric on plastic volumetric contraction .....	20
Effect of fabric on the elastic modulus.....	22
2.9- Post-shaking undrained shear strength .....	22
2.10- Post-shaking reconsolidation .....	23
2.11- Summary of constitutive equations .....	23
<b>3- Examples and Verifications .....</b>	<b>28</b>
3.1- Drained Monotonic Direct Simple Shear Tests .....	28
3.2- Undrained Monotonic Direct Simple Shear Tests .....	28
3.3- Undrained Cyclic Direct Simple Shear Tests .....	29
<b>References.....</b>	<b>41</b>

# 1- Introduction

Nonlinear seismic deformation analyses in geotechnical practice require approximating the stress-strain responses of a broad range of soil types and consistencies. Soil types can span from clearly sand-like to clearly clay-like, with a broad range of intermediate soil types that are more difficult to characterize. Soil consistency can range from loose or soft to dense or hard in natural deposits or man-made fills. The choice of engineering procedures for characterizing a soil's properties depends on its type and consistency, along with a number of project specific considerations. The choice of a constitutive model for representing a specific soil in a nonlinear dynamic analysis similarly depends on the soil type, its consistency, and a number of project-specific considerations.

The PM4Silt (version 1) plasticity model for representing low-plasticity silts and clays in geotechnical earthquake engineering applications is presented herein. The PM4Silt model builds on the framework of the stress-ratio controlled, critical state compatible, bounding surface plasticity PM4Sand model (version 3) described in Boulanger and Ziotopoulou (2015) and Ziotopoulou and Boulanger (2016). Modifications to the model were developed and implemented to improve its ability to approximate undrained monotonic and cyclic loading responses of low-plasticity silts and clays, as opposed to those for purely nonplastic silts or sands.

## 2- Model Formulation

The PM4Silt model presented herein follows the basic framework of the stress-ratio controlled, critical state compatible, bounding-surface plasticity PM4Sand (version 3) model presented by Boulanger and Ziotopoulou (2015) and Ziotopoulou and Boulanger (2016). The PM4Sand model was built on the framework provided by Dafalias and Manzari (2004).

### 2.1- Basic stress and strain terms

The basic stress and strain terms for the model are as follows. The model is based on effective stresses, with the conventional prime symbol dropped from the stress terms for convenience because all stresses are effective for the model. The stresses are represented by the tensor  $\sigma$ , the principal effective stresses  $\sigma_1$ ,  $\sigma_2$ , and  $\sigma_3$ , the mean effective stress  $p$ , the deviatoric stress tensor  $\mathbf{s}$ , and the deviatoric stress ratio tensor  $\mathbf{r}$ . The present implementation was simplified by casting the various equations and relationships in terms of the in-plane stresses only. This limits the present implementation to plane-strain applications and is not correct for general cases, but it has the advantage of simplifying the implementation and improving computational speed by reducing the number of operations. Consequently, the relationships between the various stress terms can be summarized as follows:

$$\sigma = \begin{pmatrix} \sigma_{xx} & \sigma_{xy} \\ \sigma_{xy} & \sigma_{yy} \end{pmatrix} \quad (2.1)$$

$$p = \frac{\sigma_{xx} + \sigma_{yy}}{2} \quad (2.2)$$

$$\mathbf{s} = \boldsymbol{\sigma} - p\mathbf{I} = \begin{pmatrix} s_{xx} & s_{xy} \\ s_{xy} & s_{yy} \end{pmatrix} = \begin{pmatrix} \sigma_{xx} - p & \sigma_{xy} \\ \sigma_{xy} & \sigma_{yy} - p \end{pmatrix} \quad (2.3)$$

$$\mathbf{r} = \frac{\mathbf{s}}{p} = \begin{pmatrix} r_{xx} & r_{xy} \\ r_{xy} & r_{yy} \end{pmatrix} = \begin{pmatrix} \frac{\sigma_{xx} - p}{p} & \frac{\sigma_{xy}}{p} \\ \frac{\sigma_{xy}}{p} & \frac{\sigma_{yy} - p}{p} \end{pmatrix} \quad (2.4)$$

Note that the deviatoric stress and deviatoric stress ratio tensors are symmetric with  $r_{xx} = -r_{yy}$  and  $s_{xx} = -s_{yy}$  (meaning a zero trace), and that  $\mathbf{I}$  is the identity matrix.

The model strains are represented by a tensor  $\boldsymbol{\varepsilon}$ , which can be separated into the volumetric strain  $\varepsilon_v$  and the deviatoric strain tensor  $\mathbf{e}$ . The volumetric strain is,

$$\varepsilon_v = \varepsilon_{xx} + \varepsilon_{yy} \quad (2.5)$$

and the deviatoric strain tensor is,

$$\mathbf{e} = \boldsymbol{\varepsilon} - \frac{\varepsilon_v}{3}\mathbf{I} = \begin{pmatrix} \varepsilon_{xx} - \frac{\varepsilon_v}{3} & \varepsilon_{xy} \\ \varepsilon_{xy} & \varepsilon_{yy} - \frac{\varepsilon_v}{3} \end{pmatrix} \quad (2.6)$$

In incremental form, the deviatoric and volumetric strain terms are decomposed into an elastic and a plastic part,

$$d\mathbf{e} = d\mathbf{e}^{el} + d\mathbf{e}^{pl} \quad (2.7)$$

$$d\varepsilon_v = d\varepsilon_v^{el} + d\varepsilon_v^{pl} \quad (2.8)$$

where

$d\mathbf{e}^{el}$  = elastic deviatoric strain increment tensor

$d\mathbf{e}^{pl}$  = plastic deviatoric strain increment tensor

$d\varepsilon_v^{el}$  = elastic volumetric strain increment

$d\varepsilon_v^{pl}$  = plastic volumetric strain increment

## 2.2- Critical state

The PM4Silt model uses the state parameter ( $\xi$ ) (Been and Jefferies 1985), which is the difference between the current void ratio ( $e$ ) and the critical state void ratio ( $e_{cs}$ ) at the same mean effective stress ( $p$ ). The critical state line is approximated as linear in void ratio versus natural logarithm of mean effective stress space, with a slope  $\lambda$  and intercept  $\Gamma$  when  $p' = 1$  kPa. Thus, void ratio at critical state ( $e_{cs}$ ) is related to the mean effective stress at critical state ( $p_{cs}$ ) by the following expression.

$$e_{cs} = \Gamma - \lambda \ln\left(\frac{p}{1 \text{ kPa}}\right) \quad (2.9)$$

$$\xi = e - e_{cs} \quad (2.10)$$

For silts and clays with sufficient plasticity to exhibit stress history normalization of strengths, the slope of the critical state line is often approximately parallel to the slope of the virgin consolidation line ( $C_c$ ). The value of  $C_c$  is generally taken as the slope in void ratio versus logarithm (base 10) of mean effective stress space, and thus  $C_c$  and  $\lambda$  are related as:

$$\lambda = \frac{\log(10)}{\ln(10)} C_c = 0.434 \cdot C_c \quad (2.11)$$

### 2.3- Bounding, dilatancy, and critical surfaces

The model incorporates bounding, dilatancy, and critical stress ratio surfaces. The bounding and dilatancy surfaces are functions of the state parameter, and collapse to the critical stress ratio surface when the state parameter is zero. Lode angle dependency was removed to simplify the model.

The dilatancy ( $M^d$ ) ratio is related to the critical stress ratio ( $M$ ) by the expression,

$$M^d = M \cdot \exp\left(n^d \frac{\xi}{\lambda}\right) \quad (2.12)$$

where the model parameter  $n^d$  is a positive number so that  $M^d$  is smaller than  $M$  for dense of critical states and greater than  $M$  for loose of critical states. For the present implementation, the mean normal stress  $p$  is taken as the average of the in-plane normal stresses (Equation 2.2),  $q$  is the difference in the major and minor principal in-plane stresses, and the relationship for  $M$  is reduced to

$$M = 2 \cdot \sin(\phi_{cv}) \quad (2.13)$$

where  $\phi_{cv}$  is the constant volume or critical state effective friction angle.

The bounding ( $M^b$ ) ratio has different forms for dense versus loose of critical states. For loose of critical states (i.e., the "wet" side),  $M^b$  is related to  $M$  by the expression,

$$M^b = M \cdot \exp\left(-n^{b,wet} \frac{\xi}{\lambda}\right) \quad (2.14)$$

where the model parameter  $n^{b,wet}$  is a positive number so that  $M^b$  is smaller than  $M$  on the wet side. For dense of critical states (i.e., the "dry" side),  $M^b$  is related to  $M$  by the expression,

$$M^b = M \cdot \left(\frac{1 + C_{Mb}}{\frac{p}{p_{cs}} + C_{Mb}}\right)^{n^{b,dry}} \quad (2.15)$$

$$C_{Mb} = \frac{1}{\left(\frac{M^{b,max}}{M}\right)^{1/n^{b,dry}} - 1} \quad (2.16)$$

$$M^{b,max} = 2 \cdot \sin(\phi_{max}) \quad (2.17)$$

The above expression produces  $M^b$  values that smoothly vary from equal to  $M$  at critical state (i.e.,  $p/p_{cs} = 1$ ) to a maximum value  $M^{b,max}$  at the origin (i.e.,  $p = 0$ ). The value of  $M^{b,max}$  corresponds to the maximum friction angle than can be mobilized near the origin,  $\phi_{max}$ .

For a fixed value of state parameter (with corresponding fixed values for  $p/p_{cs}$ ,  $M^d$ , and  $M^b$ ), the bounding, dilatancy, and critical stress ratio surfaces can be visualized as linear lines on a  $q$ - $p$  plot (where  $q = \sigma_1 - \sigma_3$ ) as shown in Figure 2.1 or as circular surfaces on a stress-ratio graph of  $r_{yy}$  versus  $r_{xy}$  as shown in Figure 2.2. As the model is sheared toward critical state ( $\xi = 0$ ,  $p/p_{cs} = 1$ ), the values of  $M^b$  and  $M^d$  will both approach the value of  $M$ . Thus, the bounding and dilatancy surfaces move together during shearing until they coincide with the critical state surface when the soil has reached critical state.

For soil at a fixed void ratio, the locus of points on the bounding surface in a  $q$ - $p$  plot will be curved because changes in  $p$  will correspond to changes in state parameter and  $M^b$ . This is illustrated in Figure 2.3 showing  $q/p_{cs}$  versus  $p/p_{cs}$  for points on the bounding surface for soil at a fixed void ratio. For loose of critical states (i.e.,  $p/p_{cs} > 1$ ), the locus of  $q$ - $p$  points on the bounding surface becomes flat for  $n^{b,wet} = 1.0$  and becomes steeper with decreasing values of  $n^{b,wet}$  until it follows  $M$  at the limit of  $n^{b,wet} = 0.0$ . For dense of critical states (i.e.,  $p/p_{cs} < 1$ ), the concave locus of  $q$ - $p$  points on the bounding surface is stretched outward for larger values of  $n^{b,dry}$  and pulls closer to  $M$  with decreasing values of  $n^{b,dry}$ . The functional forms for the bounding stress ratio, as illustrated in this figure, are later shown (Section 4.2) to be important for controlling undrained (i.e., constant void ratio) behaviors in monotonic and cyclic loading.

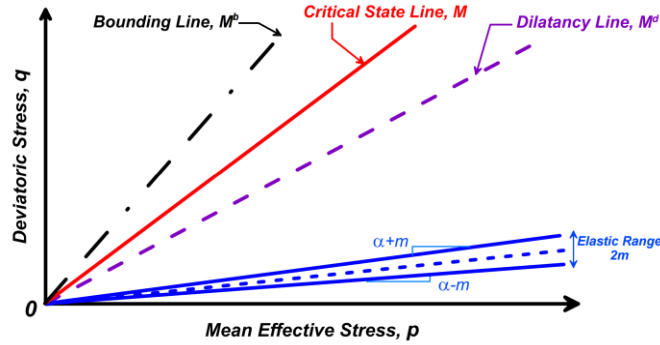


Figure 2.2. Schematic of yield, critical, dilatancy, and bounding lines in  $q$ - $p$  space for a fixed value of state parameter (after Dafalias & Manzari 2004).

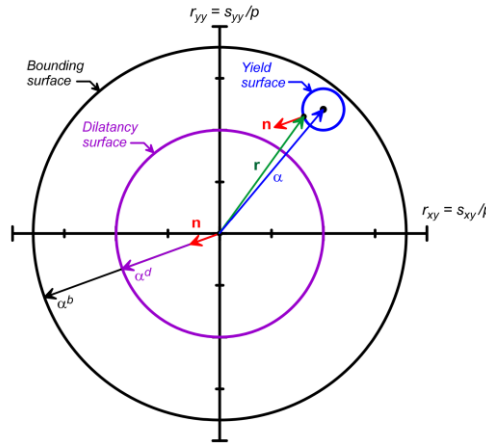


Figure 2.2. Schematic of the bounding, dilatancy, and yield surfaces on the  $r_{yy}$ - $r_{xy}$  stress-ratio plane

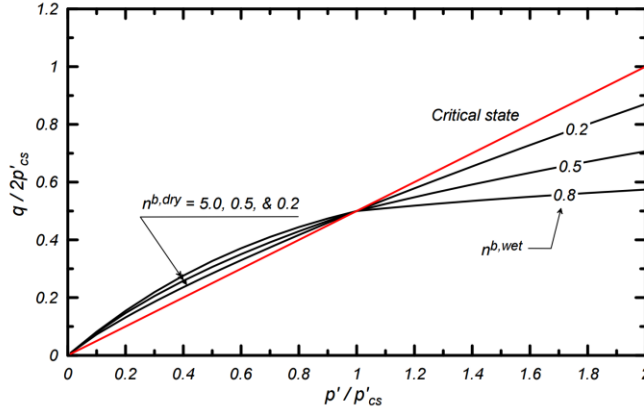


Figure 2.3. Schematic of the bounding lines and critical state line in q-p space for a fixed value of void ratio and a range of  $n^{b,dry}$  values (for dense of critical state conditions) and  $n^{b,wet}$  values (for loose of critical state conditions).

## 2.4- Yield surface and image back-stress ratio tensors

The yield surface and back-stress ratio tensor ( $\alpha$ ) follow those of the Dafalias-Manzari model, although their final form is considerably simplified by the prior assumption of removing any Lode angle dependency. The yield surface is a small cone in stress space, and is defined in stress terms by the following expression:

$$f = [(s - p\alpha):(s - p\alpha)]^{1/2} - \sqrt{1/2}pm = 0 \quad (2.18)$$

The back-stress ratio tensor  $\alpha$  defines the center of the yield surface, and the parameter  $m$  defines the radius of the cone in terms of stress ratio. The parameter  $m$  is assigned a default value of 0.01 based on results showing it provides reasonable modeling and numerical stability. The yield function can be rewritten to emphasize the role of stress ratio terms as follows,

$$f = \sqrt{(r - \alpha):(r - \alpha)} - \sqrt{1/2}m = 0 \quad (2.19)$$

The yield function can then be visualized as related to the distance between the stress ratio  $r$  and the back-stress ratio  $\alpha$ , as illustrated in Figure 2.2.

The bounding surface formulation now requires that bounding and dilatancy stress ratio tensors be defined. Dafalias and Manzari (2004) showed that it is more convenient to track back-stress ratios and to similarly define bounding and dilatancy surfaces in terms of back-stress ratios. An image back-stress ratio tensor for the bounding surface ( $\alpha^b$ ) is defined as,

$$\alpha^b = \sqrt{1/2}[M^b - m]\mathbf{n} \quad (2.20)$$

where the tensor  $\mathbf{n}$  is normal to the yield surface. An image back-stress ratio tensor for the dilatancy surface ( $\alpha^d$ ) is similarly defined as,

$$\alpha^d = \sqrt{1/2}[M^d - m]\mathbf{n} \quad (2.21)$$

The computation of constitutive responses can now be more conveniently expressed in terms of back-stress ratios rather than in terms of stress ratios, as noted by Dafalias and Manzari (2004).

## 2.5- Stress reversal and initial back-stress ratio tensors

The bounding surface formulation, as presented by Dafalias and Manzari (2004), keeps track of the initial back-stress ratio ( $\alpha_{in}$ ) and uses it in the computation of the plastic modulus  $K_p$ . This tracking of one instance in loading history is essentially a first-order method for tracking loading history. A reversal in loading direction is then identified, following traditional bounding surface practice, whenever

$$(\alpha - \alpha_{in}):n < 0 \quad (2.22)$$

A reversal causes the current stress ratio to become the initial stress ratio for subsequent loading. Small cycles of load reversal can reset the initial stress ratio and cause the plastic modulus  $K_p$  to increase accordingly, in which case the stress-strain response becomes overly stiff after a small load reversal. This is a well-known problem in bounding surface formulations for which various approaches offer different advantages and disadvantages.

The model presented herein tracks an initial back-stress ratio and a previous initial back-stress ratio ( $\alpha_{in}^p$ ), as illustrated in Figure 2.4a. When a reversal occurs, the previous initial back-stress ratio is updated to the initial back stress ratio, and the initial back-stress ratio is updated to the current back-stress ratio.

In addition, the model tracks an apparent initial back-stress ratio tensor ( $\alpha_{in}^{app}$ ) as schematically illustrated in Figure 2.4b. The schematic in Figure 2.4b is similar to that of Figure 2.4a, except that the most recent loading reversals correspond to a small unload-reload cycle on an otherwise positive loading branch. The components of  $\alpha_{in}^{app}$  are taken as: (i) for positive loading directions, the minimum value they have ever had, but no smaller than zero, and (ii) for negative loading directions, the maximum value they have ever had, but no greater than zero. These minimum and maximum past back-stress ratios are stored for each component individually and for the entire loading history. The use of  $\alpha_{in}^{app}$  helps avoid the over-stiffening of the stress-strain response following small unload-reload cycles along an otherwise monotonically increasing branch of loading, without having to track the loading history through many cycles of load reversals.

The computation of  $K_p$  utilizes the values of  $\alpha_{in}^{app}$ ,  $\alpha_{in}^{true}$ , and  $\alpha_{in}^p$ , as defined in Figure 2.4b, to better approximate the stress-strain response during an unload-reload cycle. For the last positive loading branch in this figure, the value of  $K_p$  is initially most strongly controlled (inversely) by the distance  $(\alpha - \alpha_{in}^{true}):n$ , such that the stiffness is initially large. As positive loading continues, the progressive reduction in  $K_p$  becomes increasingly dependent on  $\alpha_{in}^{app}$  as well. Once the positive loading exceeds the previous reversal point, the value of  $K_p$  becomes solely dependent on the distance  $(\alpha - \alpha_{in}^{app}):n$ . Thus, the computation of  $K_p$  has the following dependencies:

$$\begin{aligned} \text{if } (\alpha - \alpha_{in}^p):n < 0 &\Rightarrow K_p = f(\alpha_{in}^{true}, \alpha_{in}^{app}) \\ \text{else} &\Rightarrow K_p = f(\alpha_{in}^{app}) \end{aligned} \quad (2.23)$$



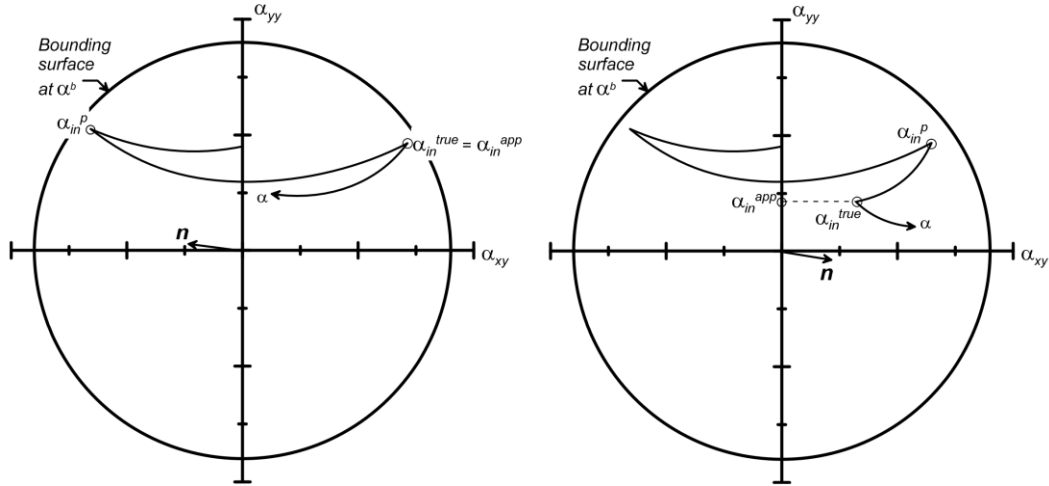


Figure 2.5. Schematic showing definitions of back-stress ratio tensors on the  $\alpha_{yy}$ - $\alpha_{xy}$  plane for: (a) a loading history with reversals in the sign of the shear stress ratios, and (b) a loading history with a recent loading reversal that does not involve reversal of the sign of the shear stress ratios.

The equations relating  $K_p$  to these back-stress ratios are given later in section 2.7.

The impact of the above logic for defining  $\alpha_{in}$  on stress-strain responses is demonstrated in Figure 2.5 showing  $\alpha_{xy}$  versus shear strain  $\gamma$  computed for two different drained DSS loading simulations. For these two examples, the reloading stiffness of the current loading branch (green line) is initially large because  $K_p$  is initially computed based on  $\alpha_{in} = \alpha_{in}^{true}$ . As the loading exceeds  $\alpha_{in}^p$ , the loading stiffness becomes much softer because  $K_p$  is now computed based on  $\alpha_{in} = \alpha_{in}^{app}$ .

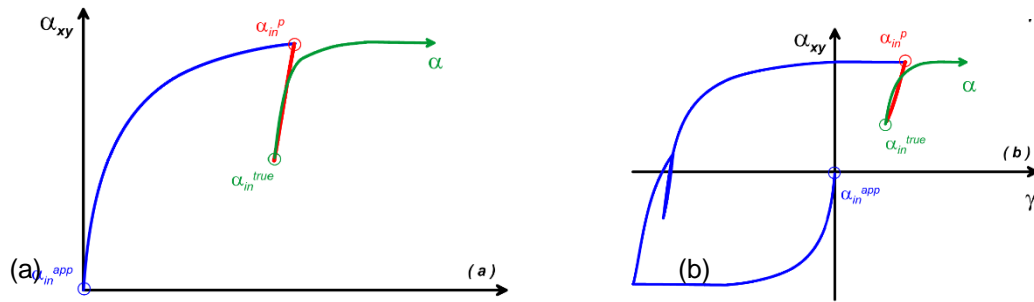


Figure 2.5. Drained DSS simulations showing  $\alpha_{xy}$  versus  $\gamma$  with the points corresponding to the current back-stress ratio  $\alpha$ , the apparent initial back-stress ratio  $\alpha_{in}^{app}$ , the true initial back-stress ratio  $\alpha_{in}^{true}$ , and the previous initial back-stress ratio  $\alpha_{in}^p$  for: (a) monotonic shearing with one intermediate unload-reload cycle, and (b) a more general sequence of cyclic loading

## 2.6- Elastic strains and moduli

The elastic deviatoric strain and elastic volumetric strain increments are computed as:

$$de^{el} = \frac{ds}{2G} \quad (2.24)$$

$$d\varepsilon_v^{el} = \frac{dp}{K} \quad (2.25)$$

where  $G$  is the elastic shear modulus and  $K$  is the elastic bulk modulus. The elastic shear modulus in the model presented herein is dependent on the mean effective stress according to,

$$G = G_o p_A \left( \frac{p}{p_A} \right)^{n_G} C_{SR} \quad (2.26)$$

where  $G_o$  and  $n_G$  are constants,  $p_A$  is the atmospheric pressure (101.3 kPa), and  $C_{SR}$  is factor that accounts for stress ratio effects (described below).

Dafalias and Manzari (2004) had included dependence of  $G$  on void. This aspect was not included in the model herein because: (1) the effects of void ratio changes on  $G$  are small relative to those of confining stress, (2) the value of  $G_o$  is more strongly affected by environmental factors such as cementation and ageing, and (3) the calibration of  $G$  to in-situ shear wave velocity data is simplified by not including  $e$ .

The CSR factor to account for stress ratio effects was included in the PM4Sand model and retained herein for the PM4Silt model. The effect of stress ratio was shown to generally be less than about 10% when the ratio of major to minor principal effective stresses is less than about 2.5, but to also increase to about 20-30% at higher principal stress ratios. They also showed that stress ratio history caused a reduction in the small-strain elastic shear modulus when the maximum previous stress ratio was greater than the current stress ratio. The effect of stress ratio and stress ratio history on the elastic shear modulus was approximately accounted for in the PM4Sand model by the factor  $C_{SR}$ . The following equation for  $C_{SR}$  represents stress ratio effects, except that it uses stress ratio terms consistent with the present model,

$$C_{SR} = 1 - C_{SR,o} \cdot \left( \frac{M}{M^b} \right)^{m_{SR}} \quad (2.27)$$

The above equation approximates Yu and Richart's (1984) results for stress ratio effects when  $C_{SR,o} = 0.3$  and  $m_{SR} = 2$ . The effects of stress ratio history would cause further reductions, and is more complicated to represent. The calibration examples for PM4Sand worked well with  $C_{SR,o} = 0.5$  and  $m_{SR} = 4$ , which keeps the effect of stress ratio on elastic modulus small at small stress ratios, but lets the effect increase to a 60% reduction when the stress ratio is on the bounding surface. The same default parameters are retained for PM4Silt, although the experimental basis for extending this relationship to low-plasticity silts and clays is lacking.

The elastic bulk modulus is related to the shear modulus through the Poisson's ratio as,

$$K = \frac{2(1 + \nu)}{3(1 - 2\nu)} G \quad (2.28)$$

as was done by Dafalias and Manzari (2004).

## 2.7- Plastic components without fabric effects

### Loading index

The loading index ( $L$ ) is used to compute the plastic component of the volumetric strain increment and the plastic deviatoric strain increment tensor as,

$$d\varepsilon_v^{pl} = \langle L \rangle D \quad (2.29)$$

$$d\mathbf{e}^{pl} = \langle L \rangle \mathbf{R}' \quad (2.30)$$

where  $D$  is the dilatancy,  $\mathbf{R}$  is the direction of  $d\mathbf{e}^{pl}$ ,  $\mathbf{R}'$  is the deviatoric component of  $\mathbf{R}$ , and  $\langle \rangle$  are MacCauley brackets that set negative values to zero [i.e.,  $\langle L \rangle = L$  if  $L \geq 0$ , and  $\langle L \rangle = 0$  if  $L < 0$ ]. The tensor  $\mathbf{R}$  for the assumption of no Lode angle dependency is,

$$\mathbf{R} = \mathbf{n} + \frac{1}{3} D \mathbf{I} \quad (2.31)$$

where  $\mathbf{n}$  is the unit normal to the yield surface (Figure 2.2). Note that the assumption of no Lode angle dependency also means that  $\mathbf{R}' = \mathbf{n}$ . The dilatancy  $D$  relates the incremental plastic volumetric strain to the absolute value of the incremental plastic deviatoric strain,

$$D = \frac{d\varepsilon_v^{pl}}{|d\mathbf{e}^{pl}|} \quad (2.32)$$

The dilatancy  $D$  can be also related to the conventional engineering shear strain in this plane strain approximation, as

$$D = \frac{d\varepsilon_v^{pl}}{\sqrt{1/2} |d\gamma^{pl}|} \quad (2.33)$$

The loading index, as derived in Dafalias and Manzari (2004) is,

$$L = \frac{1}{K_p} \frac{\partial f}{\partial \boldsymbol{\sigma}} : d\boldsymbol{\sigma} = \frac{1}{K_p} [\mathbf{n} : d\mathbf{s} - \mathbf{n} : \mathbf{r} dp] \quad (2.34)$$

$$L = \frac{2G\mathbf{n} : d\mathbf{e} - \mathbf{n} : \mathbf{r} K d\varepsilon_v}{K_p + 2G - K D \mathbf{n} : \mathbf{r}}$$

The stress increment for an imposed strain increment can then be computed as,

$$d\boldsymbol{\sigma} = 2G d\mathbf{e} + K d\varepsilon_v \mathbf{I} - \langle L \rangle (2G\mathbf{n} + K D \mathbf{I}) \quad (2.35)$$

### Hardening and the update of the back-stress ratio

Updating of the back-stress ratio is dependent on the hardening aspects of the model. Dafalias and Manzari (2004) updated the back-stress ratio according to bounding surface practice as,

$$d\boldsymbol{\alpha} = \langle L \rangle \left( \frac{2}{3} \right) h (\boldsymbol{\alpha}^b - \boldsymbol{\alpha}) \quad (2.36)$$

where  $h$  is the hardening coefficient. The factor of  $2/3$  was included for convenience so that model constants would be the same in triaxial and multi-axial derivations. They subsequently showed that the consistency condition  $\delta f = 0$  was satisfied when the plastic modulus  $K_p$  was related to the hardening coefficient as,

$$K_p = \frac{2}{3} p \cdot h \cdot (\boldsymbol{\alpha}^b - \boldsymbol{\alpha}) : \mathbf{n} \quad (2.37)$$

This expression can be rearranged so as to show that the consistency equation can be satisfied by expressing the hardening coefficient as,

$$h = \frac{3}{2} \cdot \frac{K_p}{p \cdot (\alpha^b - \alpha) : \mathbf{n}} \quad (2.38)$$

The relationship for the plastic modulus can subsequently take a range of forms, provided that the hardening coefficient and updating of the back-stress ratio follow the above expressions.

### Plastic modulus

The plastic modulus in the multi-axial generalized form of Dafalias and Manzari (2004), after substituting in their expression for the hardening coefficient, can be expressed as,

$$K_p = \frac{2}{3} G \cdot h_o \cdot \left[ \frac{1+e}{(2.97-e)^2} \cdot (1-C_h e) \right] \cdot \frac{(\alpha^b - \alpha) : \mathbf{n}}{(\alpha - \alpha_{in}) : \mathbf{n}} \quad (2.39)$$

where  $h_o$  and  $C_h$  are scalar parameters and  $e$  is the void ratio. Setting aside the secondary influence of void ratio, this form illustrates that  $K_p$  is proportional to  $G$ , proportional to the distance of the back-stress ratio to the bounding back-stress ratio, and inversely proportional to the distance of the back-stress ratio from the initial back-stress ratio.

The plastic modulus relationship was revised in the model presented herein to provide an improved approximation of empirical relationships for secant shear modulus and equivalent damping ratios during drained strain-controlled cyclic loading. The plastic modulus is computed as,

$$K_p = G \cdot h_o \cdot \frac{[(\alpha^b - \alpha) : \mathbf{n}]^{0.5}}{[\exp[(\alpha - \alpha_{in}^{app}) : \mathbf{n}] - 1] + C_{\gamma 1}} C_{rev} \quad (2.40)$$

$$C_{rev} = \frac{(\alpha - \alpha_{in}^{app}) : \mathbf{n}}{(\alpha - \alpha_{in}^{true}) : \mathbf{n}} \text{ for } (\alpha - \alpha_{in}^p) : \mathbf{n} \leq 0$$

$$= 1 \text{ otherwise} \quad (2.41)$$

The factor  $C_{rev}$  accounts for the effect of unload-reload cycles as discussed in Section 2.5 and illustrated in Figure 2.5. The constant  $C_{\gamma 1}$  in the denominator serves to avoid division by zero and has a slight effect on the nonlinearity and damping at small shear strains. If  $C_{\gamma 1} = 0$ , then the value of  $K_p$  will be infinite at the start of a loading cycle because  $(\alpha - \alpha_{in}) : \mathbf{n}$  will also be zero. In that case, nonlinearity will become noticeable only after  $(\alpha - \alpha_{in}) : \mathbf{n}$  becomes large enough to reduce  $K_p$  closer to the value of  $G$  (e.g.,  $K_p/G$  closer to 100 or 200). Setting the value of  $C_{\gamma 1} = h_o/200$  produces a reasonable response as will be demonstrated later with examples of modulus reduction and equivalent damping ratios. The stress ratio is precluded from being outside the bounding surface in the present implementation. The plastic modulus is further modified for the effects of fabric and fabric history, as described in a later section.

### Plastic volumetric strains - Dilation

Plastic volumetric strains are related to plastic deviatoric strains through the dilatancy  $D$  (Equations 2.29 and 2.30), which is computed in the Dafalias and Manzari (2004) model and the base component of the model presented herein (with additional fabric effects described in a later section) as,

$$D = A_{do} \cdot [(\alpha^d - \alpha) : \mathbf{n}] \quad (2.42)$$

Note that dilation (increasing void ratio) occurs whenever the term  $(\alpha^d - \alpha) : \mathbf{n}$  is less than zero whereas contraction (decreasing void ratio) occurs when it is positive.

For sands, the constant  $A_{do}$  in this relationship can be related to the dilatancy relationship proposed by Bolton (1986), which follows from the work of Rowe (1962), through the following sequence of steps. Bolton showed that the difference between peak and constant volume friction angles in sands could be approximated as,

$$\phi_{pk} - \phi_{cv} = -0.8\psi \quad (2.43)$$

with

$$\psi = \tan^{-1} \left( \frac{d\varepsilon_v^{pl}}{|d\gamma^{pl}|} \right) \quad (2.44)$$

Since  $\psi \approx \tan(\psi)$  for  $\psi$  less than about 0.35 radians (20 degrees), the difference between peak and constant volume friction angles (in radians) can be approximated as,

$$\phi_{pk} - \phi_{cv} = -0.8 \frac{d\varepsilon_v^{pl}}{|d\gamma^{pl}|} = -0.8 \sqrt{\frac{1}{2}} D \quad (2.45)$$

The peak friction angle is mobilized at the bounding surface, so this can be written as,

$$\begin{aligned} \phi_{pk} - \phi_{cv} &= -0.8 \sqrt{\frac{1}{2}} A_{do} \cdot [(\alpha^d - \alpha) : \mathbf{n}] \\ \phi_{pk} - \phi_{cv} &= -0.8 \sqrt{\frac{1}{2}} A_{do} \cdot \left[ \left( \frac{M^d}{\sqrt{2}} \mathbf{n} - \frac{M^b}{\sqrt{2}} \mathbf{n} \right) : \mathbf{n} \right] \end{aligned} \quad (2.46)$$

The term  $\mathbf{n} : \mathbf{n}$  is equal to unity, and the values of  $\phi_{pk}$  and  $\phi_{cv}$  (again in radians) can be replaced with expressions in terms of  $M^b$  and  $M^d$  as,

$$\sin^{-1} \left( \frac{M^b}{2} \right) - \sin^{-1} \left( \frac{M^d}{2} \right) = 0.4 A_{do} \cdot [M^b - M^d] \quad (2.47)$$

This expression can then be rearranged to solve for  $A_{do}$  as,

$$A_{do} = \frac{1}{0.4} \frac{\sin^{-1} \left( \frac{M^b}{2} \right) - \sin^{-1} \left( \frac{M^d}{2} \right)}{M^b - M^d} \quad (2.48)$$

where the angles returned by the  $\sin^{-1}$  functions are in radians.

The parameter  $A_{do}$  should thus be chosen to be consistent with the relationships that control  $M^b$  and  $M^d$ . For sands, the value for  $A_{do}$  ranged from 1.26 to 1.45 for a range of relative states and the functions used in the PM4Sand model (Boulanger and Ziotopoulou 2015). If these stress-dilatancy relationships are considered applicable for low plasticity silts and clays, then the above expression produces  $A_{do}$  values ranging from 0.8 to 1.2 for the  $M^b$  and  $M^d$  functions described herein with a wide range of values for  $n^{b,dry}$ ,  $n^d$ ,  $\xi$ , and  $\lambda$ . A default value for  $A_{do}$  of 0.8 is adopted in the PM4Silt model based on the other default parameters summarized in a later section, although an alternative value for  $A_{do}$  can be specified by the user.

## Plastic volumetric strains - Contraction

Plastic volumetric strains during contraction (i.e., whenever  $(\alpha^d - \alpha):n$  is greater than zero) are computed in the Dafalias and Manzari (2004) model using the same expression as used for dilatancy,

$$D = A_{do} \cdot [(\alpha^d - \alpha):n] \quad (2.49)$$

The use of this expression was found to limit the ability of the model to approximate a number of important loading responses; e.g., it overestimated the slope of the cyclic resistance ratio (CRR) versus number of equivalent uniform loading cycles for undrained cyclic element tests (e.g., Ziotopoulou and Boulanger 2012).

Plastic volumetric strains during contraction for the model presented herein are computed using the following expression,

$$D = A_{dc} \cdot [(\alpha - \alpha_{in}^{app}):n + C_{in}]^2 \frac{(\alpha^d - \alpha):n}{(\alpha^d - \alpha):n + C_D} \quad (2.50)$$

$$A_{dc} = \frac{A_{do}}{h_p} \quad (2.51)$$

The various forms in the above relationships were initially developed to improve different aspects of the calibrated model's performance for sands. The value of  $D$  was set proportional to the square of  $((\alpha - \alpha_{in}):n + C_{in})$  to improve the slope of the relationship between CRR and number of uniform loading cycles. The  $C_{in}$  term depends on fabric and is described in a later section along with other modifications to the above expression for the effects of fabric and fabric history. The inclusion of the term  $C_{in}$  improves the stress paths for undrained cyclic loading and the volumetric strain response during drained cyclic loading of sand; Inclusion of this constant enables some volumetric strain to develop early in the unloading from a point outside the dilatancy surface (as described later). The remaining terms on the right hand side of the equation were chosen to be close to unity over most of the loading range, while ensuring that  $D$  smoothly goes to zero as  $\alpha$  approaches  $\alpha^d$ ; reasonable results were obtained using a  $C_D$  value of 0.10.

The parameter  $A_{dc}$  for contraction was related to the value of  $A_{do}$  for dilation by dividing it by a parameter  $h_p$  that can be varied during the calibration process to obtain desired cyclic resistance ratios. The effect of varying states on cyclic loading behavior was then conveniently incorporated by making  $h_p$  depend on  $\xi/\lambda$  as follows.

$$h_p = h_{po} \cdot \exp\left(-0.7 + 0.2\left(3 - \frac{\xi}{\lambda}\right)^2\right) \quad (2.52)$$

Thus, the scalar constant  $h_{po}$  provides a linear scaling of contraction rates while the functional form of the remaining portion of this expression provides for stronger variations with state (which helps with calibration of the  $h_{po}$  values). Once the other input parameters have been selected, the constant  $h_{po}$  can be calibrated to arrive at a desired cyclic resistance ratio.

An upper limit was imposed on the contraction rate, with the limiting value computed as,

$$D \leq A_{do} \frac{(\alpha^d - \alpha):n}{(\alpha^d - \alpha):n + C_D} \quad (2.53)$$

A similar limit was used in PM4Sand to prevent numerical issues that can be encountered with excessively large contraction rates with some combinations of input parameters. For most calibrations of PM4Silt, this limit does not appear to control contraction rates.

## 2.8- Fabric effects

Dafalias and Manzari (2004) introduced a fabric-dilatancy tensor ( $\mathbf{z}$ ) that could be used to account for the effects of prior straining in sand. Their fabric tensor ( $\mathbf{z}$ ) evolved in response to plastic volumetric dilation strains, according to,

$$dz = -c_z \langle -d\varepsilon_v^{pl} \rangle (z_{max} \mathbf{n} + \mathbf{z}) \quad (2.54)$$

where the parameter  $c_z$  controls the rate of evolution and  $z_{max}$  is the maximum value that  $\mathbf{z}$  can attain.

The fabric-dilatancy tensor was modified for the present model as,

$$dz = -\frac{c_z}{1 + \langle \frac{z_{cum}}{z_{max}} - 1 \rangle} \frac{\langle -d\varepsilon_v^{pl} \rangle}{D} (z_{max} \mathbf{n} + \mathbf{z}) \quad (2.55)$$

In this expression, the tensor  $\mathbf{z}$  evolves in response to plastic deviatoric strains that occur during dilation only (i.e., dividing the plastic volumetric strain by the dilatancy gives plastic shear strain). In addition, the evolution of fabric is restricted to only occur when  $(\alpha^d - \alpha):n < 0$ ; this additional constraint precludes fabric evolution during dilation above the rotated dilatancy surface (introduced later) but below the non-rotated dilatancy surface. The parameter  $z_{cum}$  is the cumulative value of absolute changes in  $\mathbf{z}$  computed according to,

$$dz_{cum} = |dz| \quad (2.56)$$

The rate of evolution for  $\mathbf{z}$  therefore decreases with increasing values of  $z_{cum}$ , which enables the undrained cyclic stress-strain response to progressively accumulate shear strains rather than lock-up into a repeating stress-strain loop. In addition, the greatest past peak value (scalar amplitude) for  $\mathbf{z}$  during its loading history is also tracked,

$$z_{peak} = \max \left( \sqrt{\frac{\mathbf{z}:\mathbf{z}}{2}}, z_{peak} \right) \quad (2.57)$$

The values of  $\mathbf{z}$ ,  $z_{peak}$ , and  $z_{cum}$  are later used to facilitate the accumulation of shear strains under symmetric loading through their effects on the plastic modulus and dilatancy relationships.

### Additional memory of fabric formation history

Memory of the fabric formation history was included in the model presented herein to improve the ability of the model to account for the effects of sustained static shear stresses and account for differences in fabric effects for various drained versus undrained loading conditions.

The initial fabric tensor ( $\mathbf{z}_{in}$ ) at the start of the current loading path is determined whenever a stress ratio reversal occurs, and thus correspond to the same times that the initial back-stress ratio and previous initial back-stress ratio are updated. The  $\mathbf{z}_{in}$  tracks the immediate history terms without any consideration of whether an earlier loading cycle had produced greater degrees of fabric (i.e., the logic is different from that adopted for the updating of back-stress ratio history terms). This history term is used for describing the degree of stress rotation and its effects on plastic modulus, as described later.

Another aspect of the fabric history that is tracked is the mean stress at which the fabric is formed. This aspect of fabric history is tracked by tracking the product of  $\mathbf{z}$  and  $p$ , and defining  $p_{zp}$  as the mean stress at the time that this product achieves its greatest peak value. The  $p_{zp}$  is used in addressing a couple of

issues, including the issue of how fabric that is formed during cyclic loading may be erased during reconsolidation. For example, saturated soils that develop cyclic mobility behavior during undrained cyclic loading clearly remembers its history of plastic deviatoric strains and then subsequently forgets (to a large extent) this prior strain history when it reconsolidates back to its pre-earthquake confining stress. As another example, the memory of prior strains during undrained cyclic loading is very different than the memory of prior strains during drained cyclic loading. This memory conceptually could be related to the history of plastic and total volumetric strains, but a simpler method to account for this effect is to consider how the mean stress  $p$  relates to the value of  $p_{zp}$ . Conceptually, it appears that prior strain history (or fabric) is most strongly remembered when the soil is operating under mean stresses that are smaller than those that existed when the fabric was formed (i.e.,  $p \ll p_{zp}$ ) and then largely forgotten when they are of the same order (i.e.,  $p \approx p_{zp}$ ). This attribute will be used in the relationships described later for describing the effects of fabric on dilatancy.

### Effect of fabric on plastic modulus

An effect of fabric on the plastic modulus was added to the model presented herein by reducing the plastic modulus as the fabric tensor increased in peak amplitude, as follows:

$$K_p = G \cdot h_o \cdot \frac{[(\alpha^b - \mathbf{a}) : \mathbf{n}]^{0.5}}{\left[ \exp((\alpha - \mathbf{a}_{in}^{app}) : \mathbf{n}) - 1 \right] + C_{\gamma 1}} C_{rev} \cdot \frac{C_{k\alpha}}{1 + C_{Kp} \left( \frac{z_{peak}}{z_{max}} \right) \langle (\alpha^b - \mathbf{a}) : \mathbf{n} \rangle \sqrt{1 - C_{zpk2}}} \quad (2.58)$$

where,

$$C_{k\alpha} = 1 + \frac{C_{k\alpha f}}{1 + (2.5 \cdot \langle (\alpha - \mathbf{a}_{in}^{true}) : \mathbf{n} \rangle)^2} \cdot C_{pzp2} \cdot C_{zpk1} \quad (2.59)$$

$$C_{zpk1} = \frac{z_{peak}}{z_{cum} + \frac{z_{max}}{5}} \quad (2.60)$$

$$C_{zpk2} = \frac{z_{peak}}{z_{cum} + \frac{z_{max}}{100}} \quad (2.61)$$

$$C_{pzp2} = \frac{-\langle -(p_{zp} - p) \rangle}{-\langle -(p_{zp} - p) \rangle + p_{min}} \quad (2.62)$$

The above expressions produce a reduction in plastic modulus when fabric is favorable ( $\mathbf{z} : \mathbf{n} \geq 0$ ) and with increasing plastic shear strains (which conceptually would break down any cementation). This reduces both the plastic modulus and the hysteretic damping at larger shear strains (note that  $z_{peak} = 0$  unless the soil has been loaded strongly enough to pass outside the dilatancy surface), improves the volumetric strains that develop in drained cyclic loading, and improves the path in undrained cyclic loading.

The  $C_{K\alpha}$  and  $\sqrt{1 - C_{zpk2}}$  terms both serve to increase  $K_p$  during non-reversal loading by amounts that depend on the fabric and stress history. During reversal loading, the  $\sqrt{1 - C_{zpk2}}$  term approaches unity and  $K_p$  evolves as it previously had. The roles of each of the other terms are discussed below.

$C_{zpk1}$  and  $C_{zpk2}$  are terms that start from zero and grow to be unity for uni-directional growth of fabric which is the case during non-reversing loading conditions. These two terms differ by the rate under which they approach unity by the use of the constant  $z_{max}/5$  or  $z_{max}/100$  with these respective values chosen for their



ability to better approximate the engineering behaviors of interest. For full reversal loading where the fabric alternates between positive and negative values, these terms will both go to zero.

$C_{pzp2}$  starts initially at zero and stays equal to zero until fabric is formed. After fabric is formed, this term quickly transitions to unity for values of mean effective stress  $p$  that are less than the value that  $p$  had when the maximum fabric was formed ( $p_{zp}$ ). If  $p$  increases beyond the value of  $p_{zp}$  the term will return to zero according to the MacCauley brackets.

The values for the calibration parameters  $C_{Kp}$  and  $C_{Kaf}$  were chosen for their ability to reasonably approximate the targeted behaviors, as discussed later. Setting  $C_{Kp}$  to a default value of 2.0 was found to produce reasonable responses for sand with particular emphasis on improving (reducing) the equivalent damping ratios at shear strains of 1 to 3% in drained cyclic loading; the same default value for  $C_{Kp}$  was retained for PM4Silt. The parameter  $C_{Kaf}$  was useful for adjusting the undrained cyclic loading response with sustained static shear stresses for sands. For PM4Silt, the  $C_{Kaf}$  term has little effect on cyclic strengths for soils that are loose-of-critical, but does become more influential for dense-of-critical soils. For the present implementation of PM4Silt, a default value of 4.0 was adopted regardless of initial state.

The cumulative effect of the above parameters can be understood as follows. If a soil is strongly loaded in uni-directional loading and forms significant amount of fabric and is then unloaded, then upon subsequent reloading the terms  $C_{pzp2}$  and  $C_{zpk1}$  will be unity and  $C_{K\alpha}$  will become large. If the loads are increased to where the soil is being sheared and forming fabric at even higher stresses (higher values of  $p$  than fabric was previously formed at) then  $C_{K\alpha}$  will be unity ( $C_{pzp2} = 0$ ). In this way, an element that has developed strong fabric under monotonic or cyclic loading without reversal of the total shear stress direction (e.g., an element within a steep slope where the static shear stresses are greater than the cyclic shear stresses) will, when unloaded and reloaded, be initially much stiffer (increased  $K_p$ ) followed by a softening (smaller  $K_p$ ) if the soil is loaded into virgin territory.

### Effect of fabric on plastic volumetric dilation

A rotated dilatancy surface with slope  $M^{dR}$  which evolves with the history of the fabric tensor  $\mathbf{z}$  was added to the framework of the model to facilitate earlier dilation at low stress ratios under certain loading paths for sands (Ziotopoulou and Boulanger 2015).

The rotated surface is equal to the original dilatancy surface scaled-down by a factor  $C_{rot1}$ :

$$M^{dR} = \frac{M^d}{C_{rot1}} \quad (2.63)$$

$$C_{rot1} = 1 + \frac{2 \cdot \langle -\mathbf{z} : \mathbf{n} \rangle}{\sqrt{2} z_{max}} \cdot (1 - C_{zin1}) \geq 1 \quad (2.64)$$

where  $M^d$  is the slope of the unrotated dilatancy surface. Experimental results (Ziotopoulou and Boulanger 2015) indicate that the loading history, the loading direction and the loading pattern play important roles in the response of sand to irregular cyclic loading. Thus the scaling factor that defines the rotated dilatancy surface was made dependent on whether fabric is favorable ( $\mathbf{z} : \mathbf{n} > 0$ ) or unfavorable ( $\mathbf{z} : \mathbf{n} < 0$ ) and on the factor  $C_{zin1}$  which is an indirect measure of whether there are reversals or not:

$$C_{zin1} = \langle 1 - \exp \left( -2.0 \left| \frac{z_{in} : \mathbf{n} - z : \mathbf{n}}{z_{max}} \right| \right) \rangle \quad (2.65)$$

where  $\mathbf{z}_{in}$  is the fabric tensor at the beginning of the current loading branch.  $C_{zin1}$  can take values ranging from 0, when there are no reversals, to 1, when there are reversals. The rotated dilatancy surface is operating only for loading with an unfavorable fabric since the factor  $C_{rot1}$  becomes 1 when the fabric is favorable (i.e.,  $\langle -\mathbf{z} : \mathbf{n} \rangle = 0$ ). In the present model, rotation of the dilatancy surface was also restricted to the case where the soil is dense of critical state (i.e.,  $C_{rot1} = 1$  for  $\xi > 0$ ).

A back-stress ratio tensor for the rotated dilatancy surface ( $\alpha^{dR}$ ) was introduced as:

$$\alpha^{dR} = \frac{1}{\sqrt{2}} \cdot (M^{dR} - m)\mathbf{n} \quad (2.66)$$

Dilation occurs whenever the term  $(\alpha^{dR} - \alpha) : \mathbf{n}$  is negative whereas contraction occurs when it is positive. The calculation of D is still treated separately during dilation and contraction.

D during dilation is now computed according to the following expressions. First, a value for D is computed from the rotated dilatancy surface:

$$D_{rot} = A_d \cdot \frac{\langle -\mathbf{z} : \mathbf{n} \rangle}{\sqrt{2}z_{max}} \cdot \frac{(\alpha^{dR} - \alpha) : \mathbf{n}}{C_{DR}} \quad (2.67)$$

where the  $C_{DR}$  factor is applied to reduce the rate under which dilatancy is increasing and is discussed further below. Second, another value for D is computed that would be obtained from the non-rotated dilatancy surface:

$$D_{non-rot} = A_d \cdot [(\alpha^d - \alpha) : \mathbf{n}] \quad (2.68)$$

The Macaulay brackets in the above expression ensure that  $D_{non-rot}$  is equal to zero whenever  $(\alpha^d - \alpha) : \mathbf{n} > 0$  while  $(\alpha^{dR} - \alpha) : \mathbf{n} < 0$ . Lastly, the operating value of D is selected from the above two values based on:

$$\begin{aligned} & \text{if } D_{non-rot} < D_{rot} \Rightarrow D = D_{non-rot} \\ & \text{else } D = D_{non-rot} + (D_{rot} - D_{non-rot}) \cdot \frac{\langle M^b - M^{cur} \rangle}{\langle M^b - M^{cur} + 0.01 \rangle} \end{aligned} \quad (2.69)$$

The above logic is illustrated in Figure 2.6 where D is plotted for a half cycle of loading that goes from contraction to dilation. This figure shows that  $D_{non-rot}$  is used whenever it is smaller (more negative) than  $D_{rot}$ . For cases where  $D_{rot}$  is smaller than  $D_{non-rot}$ , the value of D is interpolated based on the additional term on the right that multiplies the difference between  $D_{rot}$  and  $D_{non-rot}$ . This interpolation term is close to unity for stress ratios away from the bounding surface ( $M^{cur} < M^b$ ), such that D will be equal to  $D_{rot}$  as illustrated in the figure. However, this term will also go smoothly to zero as the stress ratio gets close to the bounding surface, so that dilatancy smoothly goes to zero as a soil approaches the critical state where  $M = M^d = M^b$ . The constant of 0.01 in the denominator controls the rate under which D goes to zero as the stress ratio nears the bounding surface and was found to provide reasonable results in trial simulations.

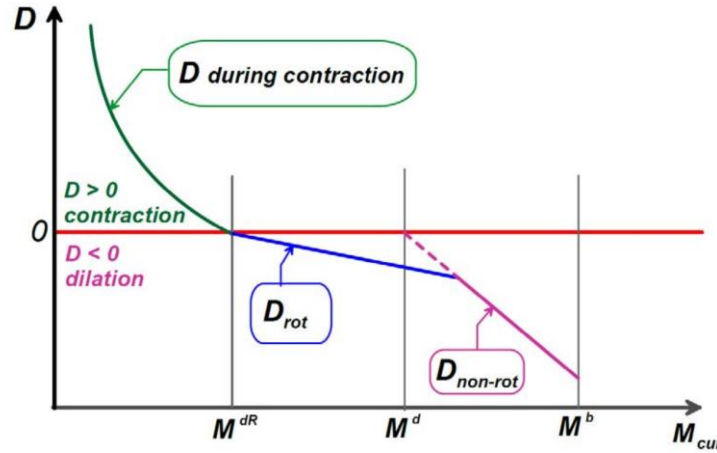


Figure 2.6. Schematic of the dilatancy  $D$  calculation based on the stress state with regards to the rotated dilatancy ( $M^{dR}$ ), dilatancy ( $M^d$ ) and bounding ( $M^b$ ) surfaces during a half-cycle of loading that goes from contraction to dilation

The factor  $C_{DR}$  in the denominator of the expression for  $D_{rot}$  is applied so that the  $D$  computed based on the rotated dilatancy surface is consistent with experimental observations. A value of 3.0 was used for the default calibration described later and found to provide reasonable results in trial simulations.

Lastly, the parameter  $A_d$  in the expressions for both  $D_{rot}$  and  $D_{non-rot}$  is expressed as,

$$A_d = \frac{A_{do}(C_{zin2})}{\left(\frac{z_{cum}^2}{z_{max}}\right) \left(1 - \frac{\langle -z : \mathbf{n} \rangle}{\sqrt{2} \cdot z_{peak}}\right)^3 (C_\varepsilon)^2 (C_{pzp})(C_{pmin})(C_{zin1}) + 1} \quad (2.70)$$

$$C_{pzp} = \frac{1}{1 + \left(2.5p/p_{zp}\right)^5} \quad (2.71)$$

$$C_{zin1} = 1.0 - \exp\left(-2.0 \left|\frac{\mathbf{z}_{in} : \mathbf{n} - \mathbf{z} : \mathbf{n}}{z_{max}}\right|\right) \quad (2.72)$$

$$C_{zin2} = \frac{1 + C_{zin1} \frac{z_{cum} - z_{peak}}{3z_{max}}}{1 + 3 \cdot C_{zin1} \frac{z_{cum} - z_{peak}}{3z_{max}}} \quad (2.73)$$

Consider the five terms added to the denominator of the expression for  $A_d$ . The first term  $[z_{cum}^2/z_{max}]$  facilitates the progressive growth of strains under symmetric loading by reducing the dilatancy that occurs when a liquefied soil has been sheared through many cycles of loading; note that this term progressively increases with subsequent cycles of loading. The second term facilitates strain-hardening when the plastic shear strain reaches the prior peak value, wherein the term approaches zero (i.e., when  $\mathbf{z} : \mathbf{n}$  approaches  $z_{peak}/\sqrt{2}$ ) and the dilation rate consequently rapidly approaches the virgin loading value of  $A_{do}$ . The third term  $C_\varepsilon$  is a calibration constant that can be used to modify the rate of plastic shear strain accumulation. The fourth term  $C_{pzp}$  causes the effects of fabric on dilation to be diminished (erased) whenever the current value of  $p$  is near the value of  $p_{zp}$ ; this term enables the model to provide

reasonable predictions of responses to large numbers of either drained or undrained loading cycles. The fifth term  $C_{zin1}$  facilitates strain-hardening when stress reversals are not causing fabric changes; i.e., when the initial and current fabric terms are close to equal, the term  $C_{zin1}$  goes to zero. Lastly, the second term in the numerator,  $C_{zin2}$ , causes the dilatancy to be decreased by up to a factor of 3 under conditions of large strains and full stress (and fabric) reversals, which improves the prediction of cyclic strain accumulation during undrained cyclic loading.

An additional constraint is placed on  $D$  during dilation at very low effective stresses. For  $p < 2p_{min}$ , the value of  $D$  cannot be smaller in magnitude than computed by the following expression:

$$D = -3.5A_{do}(M^b - M^d) \frac{2p_{min} - p}{p_{min}} \text{ for } p_{min} \leq p \leq 2p_{min} \quad (2.74)$$

This expression ensures that the model will, for dense of critical soils (i.e.,  $M^b > M^d$ ), be dilative when  $p$  falls below  $2p_{min}$ .

The parameter  $p_{min}$  is set one of two ways. If the input parameter  $r_{u,max}$  is specified, then  $p_{min}$  is computed from the value of  $p$  at the time of "consolidation" (i.e., the  $p$  value when the flag FirstCall – see Section 3 – was last set equal to 0) as:

$$p_{min} = (1 - r_{u,max}) \frac{p}{2} \quad (2.75)$$

The parameter  $r_{u,max}$  is limited to a maximum value of 0.99 and a minimum value of zero. For example, setting  $r_{u,max}$  equal to 0.95 results in  $p_{min}$  being 2.5% of the value of  $p$  at consolidation. If  $r_{u,max}$  is not specified,  $p_{min}$  is set equal to  $p_{cs}/8$ , where  $p_{cs}$  is the value of  $p$  at critical state for the specified  $s_u$ . This default relation can be expressed as,

$$p_{min} = \frac{p_{cs}}{8} = \frac{2s_u}{8M} \quad (2.76)$$

The  $p_{min}$  value obtained using this latter expression is limited to be no greater than the  $p_{min}$  computed using  $r_{u,max} = 0$ . For either case,  $p_{min}$  is further limited to be no smaller than 0.5 kPa.

### Effect of fabric on plastic volumetric contraction

Dafalias and Manzari (2004) used the fabric tensor to modify the dilatancy during contraction ( $D > 0$ ) as follows,

$$D = A_d \cdot [(\alpha^d - \alpha):n](1 + \langle z:n \rangle) \quad (2.77)$$

This relationship enhances the volumetric contraction whenever the fabric is favorable ( $\langle z:n \rangle \geq 0$ ), based on the term  $1 + \langle z:n \rangle$  as recommended by Dafalias and Manzari (2004).

The effect of fabric on dilatancy during contraction was modified for the present model as,

$$D = A_{dc} \cdot [(\alpha - \alpha_{in}^{app}):n + C_{in}]^2 \frac{(\alpha^d - \alpha):n}{(\alpha^d - \alpha):n + C_D} C_{pmin2} \quad (2.78)$$

$$A_{dc} = \frac{A_{do}(1 + \langle z:n \rangle)}{h_p C_{dz} C_{wet}} \quad (2.79)$$

$$C_D = 0.1 \quad (2.80)$$

$$C_{in} = \frac{2 \cdot \langle z:n \rangle}{\sqrt{2} z_{max}} \quad (2.81)$$

$$C_{dz} = \left( 1 - C_{rot2} \cdot \frac{\sqrt{2}z_{peak}}{z_{max}} \right) \cdot \left( \frac{z_{max}}{z_{max} + C_{rot2} \cdot z_{cum}} \right) \quad (2.82)$$

$$C_{rot2} = 1 - \frac{z_{peak}}{z_{cum} + \frac{z_{max}}{100}} (= 1 - C_{zpk2}) \quad (2.83)$$

$$C_{wet} = \frac{1}{\frac{1}{1 + \left( \frac{C_{w1}}{(\alpha^b - \alpha):n} \right)^4} + \frac{1}{1 + \left( \frac{\xi/\lambda}{C_{w2}} \right)^2}} \leq 1 \quad (2.84)$$

$$C_{w1} = 0.02 \quad (2.85)$$

$$C_{w2} = 0.1 \quad (2.86)$$

$$\begin{aligned} C_{pmin2} &= 0 \quad \text{for } p < 2p_{min} \\ &= 1 \quad \text{for } p > 8p_{min} \\ &= \frac{p - 2p_{min}}{6p_{min}} \quad \text{otherwise} \end{aligned} \quad (2.87)$$

The factor  $C_{in}$  in the expression for  $D$  has been modified so it now depends on fabric;  $C_{in}$  is zero for unfavorable fabric, and increases with increasing  $z:n$  for favorable fabric to enhance the contraction rate at the start of an unloading cycle (note that  $D$  would be zero at the start of an unloading cycle if  $C_{in}$  was zero).

The term  $C_{dz}$  in the denominator of the expression for  $A_{dc}$  serves to increase the rate of contraction as  $z_{peak}$  nears  $z_{max}$  or as a large amount of cumulative fabric formation/destruction has taken place. This term was developed for improved modeling of the cyclic strength of denser sands, for which the value of  $h_p$  can be on the order of 100 (Boulanger and Ziotopoulou 2015). The degrading of the denominator as  $z_{peak}$  or  $z_{cum}$  increases enables the generation of high excess pore pressures at higher loading levels on stronger soils, and influences the slope of the CRR versus number of uniform loading cycles relationship obtained for undrained element loading. Note that the denominator degrades whether fabric is favorable or not, but that the overall rate of contraction is more enhanced if the fabric is favorable ( $z:n \geq 0$ ). The factor  $C_{rot2}$  was introduced into the factor  $C_{dz}$  to provide better control over the rate of contraction as  $z_{peak}$  nears  $z_{max}$  or as a large amount of cumulative fabric formation/destruction has taken place. The factor  $C_{rot2}$  takes values that range from 1 for loading with zero fabric or cyclic loading that causes reversals of fabric (since  $z_{cum}$  will become much larger than  $z_{peak}$ ), to 0 for loading that causes fabric to grow monotonically in one direction such as in non-reversal cyclic loading (since  $z_{cum}$  will equal  $z_{peak}$ ).

The term  $C_{wet}$  in the denominator of the expression for  $A_{dc}$  serves to increase the rate of contraction when the stress state reaches the bounding surface for loose-of-critical state conditions. This term approaches zero for soils that are loose of critical and on the bounding surface, but increases to unity for soils that are sufficiently close to critical state (controlled by the constant  $C_{w1}$ ) or sufficiently away from the bounding surface (controlled by the constant  $C_{w2}$ ). The constants  $C_{w1}$  and  $C_{w2}$  were set to 0.02 and 0.1 because they produced reasonable responses for a range of calibrations.

The last parameter  $C_{pmin}$  varies linearly with  $p$  between values of  $C_{pmin} = 0.0$  for  $p \leq 2p_{min}$  and  $C_{pmin} = 1.0$  for  $p \geq 8p_{min}$ . This parameter provides the mechanism for limiting the maximum excess pore water

pressure ratio (or minimum effective stress) that develops during cyclic loading. When  $p$  reaches  $2p_{\min}$ , the contraction rate goes to zero such that further reductions in  $p$  will not occur during undrained loading.

### Effect of fabric on the elastic modulus

The elastic shear modulus and elastic bulk modulus may degrade with increasing values of cumulative plastic deviator strain term,  $z_{cum}$ . This component of the model was added to account for the progressive destruction, with increasing plastic shear strains, of any minor cementation bonds or other ageing- or strain history-related phenomena that produced an increase in small-strain shear modulus. The destruction of minor cementation by plastic shear strains is evidenced in the field by measurements of shear wave velocities in sand that are lower after earthquake shaking than before earthquake shaking (e.g., Arai 2006). The degradation of the elastic shear modulus is computed as,

$$G = G_o p_A \left( \frac{p}{p_A} \right)^{1/2} C_{SR} \left( \frac{1 + \frac{z_{cum}}{z_{max}}}{1 + \frac{z_{cum}}{z_{max}} C_{GD}} \right) \quad (2.88)$$

where  $C_{GD}$  is the factor by which the shear modulus is degraded (divided) at very large values of  $z_{cum}$ . This change in the elastic shear modulus  $G$  causes the bulk modulus  $K$  to progressively decrease with increasing  $z_{cum}$ . The change in  $K$  improves the model's ability to track the stress-strain response of liquefying soils. In particular, decreasing  $K$  with increasing  $z_{cum}$  reduces the rate of strain-hardening after phase transformation at larger shear strain levels, and improves the ability to approximate the hysteretic stress-strain response of a soil as it liquefies or cyclically softens.

## 2.9- Post-shaking undrained shear strength

The value of  $s_u$  that should be used for evaluating static stability after strong shaking is often smaller than used for evaluating dynamic responses for two primary reasons. First, the  $s_u$  of low plasticity silts and clays generally exhibit strain rate dependence, such that the value for post-shaking stability should correspond to the slower strain rate associated with static stability (i.e.,  $s_{u,static}$ ). Secondly, the  $s_u$  can be reduced by cyclic degradation or remolding that occurs during strong shaking.

The ability to reduce  $s_u$  at a specific time during an analysis (e.g., after the end of strong shaking) was incorporated into PM4Silt as a pragmatic means for evaluating post-shaking static stability. After strong shaking has ended, the input parameter  $F_{su}$  can be used to shift the critical state line leftward relative to its initial position by a factor of  $F_{su}$ , thereby reducing the undrained shear strength at critical state ( $s_{u,cs}$ ) by the same factor for the post-strong-shaking portion of the analysis. This shift in the critical state line can be expressed in the calculation of the state parameter as follows.

$$\xi = e - \left[ \Gamma - \lambda \cdot \ln \left( \frac{p}{F_{su} \cdot 1kPa} \right) \right] \quad (2.89)$$

The default value for  $F_{su}$  is 1.0 (no shift in the critical state line), and the code does not require that a value for  $F_{su}$  be specified during the analysis. The use of  $F_{su}$  is discussed further in Section 4.

## 2.10- Post-shaking reconsolidation

Volumetric strains that develop during reconsolidation of liquefied sands or cyclically-softened silts and clays are difficult to numerically model using the conventional constitutive separation of strains into elastic and plastic components, plus the present model is not formulated to model yielding along reconsolidation paths (e.g., constant  $K_0$  loading). The PM4Silt model retains the form of the PM4Sand model for better estimating reconsolidation strains during the post-shaking portion of a numerical simulation. The modification involved the pragmatic approach of reducing the post-shaking elastic shear modulus  $G$  (and hence elastic bulk modulus  $K$ ) which increases reconsolidation strains, thereby compensating for limitations in the model formulation. The user may activate this feature after the end of strong shaking, such that post-liquefaction reconsolidation strains are better approximated in the remainder of the simulation. This feature should not be activated for the strong shaking portion of a simulation.

The post-shaking elastic moduli are determined by multiplying the conventional elastic moduli (computed using the expressions described earlier) by a reduction factor  $F_{consol}$  as,

$$G_{post-shaking} = F_{consol} G \quad (2.90)$$

$$K_{post-shaking} = F_{consol} K \quad (2.91)$$

The  $F_{consol}$  value is computed as,

$$G_{c,min} = \left(\frac{8p}{\lambda}\right) \left( \frac{1}{1 + (C_{GC} - 1) \left( \frac{z_{cum}}{z_{cum} + z_{max}} \right)} \right) \quad (2.92)$$

$$F_{consol} = 1 - \left(1 - \frac{G_{c,min}}{G}\right) \left(1 - \frac{M^{cur}}{M^d}\right)^{0.25} \quad (2.93)$$

where the parameter  $C_{GC}$  determines how much the elastic moduli will be degraded by if  $z_{cum}$  becomes large. If  $z_{cum}$  is small, the value of  $G_{c,min}$  corresponds to an elastic modulus consistent with the one dimensional recompression stiffness estimated based on  $p$  and  $\lambda$ . Lastly, the expression for  $F_{consol}$  will return values close to  $G_{c,min}$  if the loading is well within the dilatancy surface ( $M^{cur} \ll M^d$ ) and close to  $G$  if the loading is near the dilatancy surface ( $M^{cur} \approx M^d$ ).

## 2.11- Summary of constitutive equations

The constitutive equations for the model presented herein are summarized in Table 2.1.

<b>PM4Silt model</b>	
<b>Critical state line</b>	
$\xi = e - \Gamma + \lambda \cdot \ln\left(\frac{p}{F_{su} \cdot 1kPa}\right)$	
$F_{su} = 1.0$ at initialization	
<b>Elastic deviatoric strain increment</b>	
$de^{el} = \frac{ds}{2G}$	

$$G = G_o p_A \left( \frac{p}{p_A} \right)^{1/2} C_{SR} \left( \frac{1 + \frac{z_{cum}}{z_{max}}}{1 + \frac{z_{cum}}{z_{max}} C_{GD}} \right)$$

$$C_{SR} = 1 - C_{SR,o} \cdot \left( \frac{M}{M^b} \right)^{m_{SR}}$$

$$C_{SR,o} = 0.5$$

$$m_{SR} = 4$$

### **Elastic volumetric strain increment**

$$d\varepsilon_v^{el} = \frac{dp}{K}$$

$$K = \frac{2(1+\nu)}{3(1-2\nu)} G$$

### **Yield surface**

$$f = [(s - p\alpha):(s - p\alpha)]^{1/2} - \sqrt{1/2} pm = 0$$

$$m = 0.01$$

### **Plastic deviatoric strain increment**

$$de^{pl} = \langle L \rangle R'$$

$$R = R' + \frac{1}{3} DI = n + \frac{1}{3} DI$$

$$M^b = M \cdot \exp\left(-n^{b,wet} \frac{\xi}{\lambda}\right) \text{ for } \xi \geq 0$$

$$= M \cdot \left( \frac{1 + C_{Mb}}{\frac{p}{p_{cs}} + C_{Mb}} \right)^{n^{b,dry}} \text{ for } \xi < 0$$

$$M = 2 \cdot \sin(\phi_{cv})$$

$$C_{Mb} = \frac{1}{\left( \frac{M^{b,max}}{M} \right)^{1/n^{b,dry}} - 1}$$

$$M^{b,max} = 2 \cdot \sin(\phi_{max})$$

$$\alpha^b = \sqrt{1/2} [M^b - m] n$$

$$K_p = G \cdot h_o \cdot \frac{[(\alpha^b - a):n]^{0.5}}{[\exp((\alpha - a_{in}^{app}):n) - 1] + C_{r1}} C_{rev} \cdot \frac{C_{k\alpha}}{1 + C_{Kp} \left( \frac{z_{peak}}{z_{max}} \right) ((\alpha^b - a):n) \sqrt{1 - C_{zpk2}}}$$

$$C_{rev} = \frac{(\alpha - a_{in}^{app}):n}{(\alpha - a_{in}^{true}):n} \text{ for } (\alpha - \alpha_{in}^p):n \leq 0$$

$$= 1 \text{ otherwise}$$



$$C_{k\alpha} = 1 + \frac{C_{k\alpha f}}{1 + (2.5 \cdot \langle (\alpha - \alpha_{in}^{true}) : \mathbf{n} \rangle)^2} \cdot C_{pzp2} \cdot C_{zpk1}$$

$$C_{zpk1} = \frac{z_{peak}}{z_{cum} + \frac{z_{max}}{5}}$$

$$C_{zpk2} = \frac{z_{peak}}{z_{cum} + \frac{z_{max}}{100}}$$

$$C_{pzp2} = \frac{-\langle (p_{zp} - p) \rangle}{-\langle (p_{zp} - p) \rangle + p_{min}}$$

$$C_{\gamma 1} = \frac{h_o}{200}$$

$$C_{kp} = 2$$

### **Plastic volumetric strain increment**

$$d\varepsilon_v^{pl} = \langle L \rangle D$$

$$M^d = M \cdot \exp\left(n^d \frac{\xi}{\lambda}\right)$$

$$M^{dR} = \frac{M^d}{C_{rot1}}$$

$$C_{rot1} = 1 + \frac{2 \cdot \langle -z : \mathbf{n} \rangle}{\sqrt{2} z_{max}} \cdot (1 - C_{zin1}) \geq 1$$

$$C_{zin1} = \langle 1 - \exp\left(-2.0 \left| \frac{z_{in} \cdot \mathbf{n} - z : \mathbf{n}}{z_{max}} \right| \right) \rangle$$

$$\alpha^d = \frac{1}{\sqrt{2}} \cdot (M^d - m) \mathbf{n}$$

$$\alpha^{dR} = \frac{1}{\sqrt{2}} \cdot (M^{dR} - m) \mathbf{n}$$

If dilating ( $D < 0$ ):

$$D_{non-rot} = A_d \cdot [(\alpha^d - \alpha) : \mathbf{n}]$$

$$D_{rot} = A_d \cdot \frac{\langle -z : \mathbf{n} \rangle}{\sqrt{2} z_{max}} \cdot \frac{(\alpha^{dR} - \alpha) : \mathbf{n}}{C_{DR}}$$

$$\text{if } D_{non-rot} < D_{rot} \Rightarrow D = D_{non-rot}$$

$$\text{else } D = D_{non-rot} + (D_{rot} - D_{non-rot}) \cdot \frac{\langle M^b - M^{cur} \rangle}{\langle M^b - M^{cur} + 0.01 \rangle}$$

$$A_d = \frac{A_{do}(C_{zin2})}{\left(\frac{z_{cum}^2}{z_{max}}\right) \left(1 - \frac{\langle -z : \mathbf{n} \rangle}{\sqrt{2} z_{peak}}\right)^3 (C_\varepsilon)^2 (C_{pzp})(C_{pmin})(C_{zin1}) + 1}$$

$$A_{do} = \frac{1}{0.4} \cdot \frac{\left[\sin^{-1}\left(\frac{M^b}{2}\right) - \sin^{-1}\left(\frac{M}{2}\right)\right]}{M^b - M^d}$$

$$C_{pzp} = \frac{1}{1 + \left(2.5p/p_{zp}\right)^5}$$

$$C_{pmin} = \frac{1}{1 + (p_{min2}/p)^2}$$

$$C_{zin1} = 1.0 - \exp\left(-2.0 \left| \frac{z_{in:n} - z:n}{z_{max}} \right| \right)$$

$$C_{zin2} = \frac{1 + C_{zin1} \frac{z_{cum} - z_{peak}}{3z_{max}}}{1 + 3C_{zin1} \frac{z_{cum} - z_{peak}}{3z_{max}}}$$

$$C_{DR} = 3.0$$

If contracting ( $D \geq 0$ )

$$D = A_{dc} \cdot [(\alpha - \alpha_{in}^{app}):n + C_{in}]^2 \frac{(\alpha^d - \alpha):n}{(\alpha^d - \alpha):n + C_D} C_{pmin2} \leq A_{do} \frac{(\alpha^d - \alpha):n}{(\alpha^d - \alpha):n + C_D} C_{pmin2}$$

$$A_{dc} = \frac{A_{do}(1 + \langle z:n \rangle)}{h_p C_{dz} C_{wet}}$$

$$C_{in} = \frac{2 \cdot \langle z:n \rangle}{\sqrt{2} z_{max}}$$

$$C_{dz} = \left(1 - C_{rot2} \cdot \frac{\sqrt{2} z_{peak}}{z_{max}}\right) \cdot \left(\frac{z_{max}}{z_{max} + C_{rot2} \cdot z_{cum}}\right)$$

$$C_{rot2} = 1 - \frac{z_{peak}}{z_{cum} + \frac{z_{max}}{100}} (= 1 - C_{zpk2})$$

$$C_D = 0.1$$

$$C_{wet} = \frac{1}{\frac{1}{1 + \left(\frac{C_{w1}}{(\alpha^b - \alpha):n}\right)^4} + \frac{1}{1 + \left(\frac{\xi/\lambda}{C_{w2}}\right)^2}} \leq 1$$

$$C_{w1} = 0.02$$

$$C_{w2} = 0.1$$

$$h_p = h_{po} \cdot \exp\left(-0.7 + 0.2 \left(3 - \frac{\xi}{\lambda}\right)^2\right) \text{ for } \frac{\xi}{\lambda} \leq 3$$

$$h_p = h_{po} \cdot \exp(-0.7) \text{ for } \frac{\xi}{\lambda} > 3$$

If  $p < 2p_{min}$

$$D = -3.5 A_{do} \langle M^b - M^d \rangle \frac{2p_{min} - p}{p_{min}}$$

**Fabric-dilatancy tensor update if  $(\alpha^d - \alpha):n < 0$**

$$dz = - \frac{c_z}{1 + \left(\frac{z_{cum}}{z_{max}} - 1\right)} \frac{\langle -d\varepsilon_v^{pl} \rangle}{D} (z_{max} \mathbf{n} + \mathbf{z})$$

$$dz_{cum} = |dz|$$

**Stress increment**

$$L = \frac{2Gn:de - n:rKd\varepsilon_v}{K_p + 2G - K D n:r}$$

$$d\sigma = 2Gde + Kd\varepsilon_v \mathbf{I} - \langle L \rangle (2G\mathbf{n} + KDI)$$

### ***Post-shaking reconsolidation***

$$G_{post-shaking} = F_{consol}G$$

$$K_{post-shaking} = F_{consol}K$$

$$G_{c,min} = \left(\frac{8p}{\lambda}\right) \left( \frac{1}{1+(C_{GC}-1)\left(\frac{z_{cum}}{z_{cum}+z_{max}}\right)} \right)$$

$$F_{consol} = 1 - \left(1 - \frac{G_{c,min}}{G}\right) \left(1 - \frac{M^{cur}}{M^d}\right)^{0.25}$$

## 3- Examples and Verifications

The PM4Silt primary model parameters consists of four main properties. The rest of model parameters have default values that automatically can be assigned to or calculated for them. In RS2 the later set of parameters have their default values in their dialog field or have “Auto Calculate” option. The users have the option of choosing the default values for these variables or change them as they would see fit.

The four primary input properties are the undrained shear strength at critical state ( $s_u$ ) or the corresponding undrained shear strength ratio ( $s_u/\sigma'_{vc}$ ), the shear modulus coefficient ( $G_o$ ), the contraction rate parameter ( $h_{po}$ ), and the post-shaking shear strength reduction factor ( $F_{su}$ ). The first three are required parameters, whereas the fourth is optional.

For the purpose of verification series of simulations are considered that include Drained Direct Simple Shear Test, Undrained Direct Simple Shear Test and Undrained Cyclic Direct Simple Shear Tests. The primary parameters of the loose, medium dense and dense sands are presented in table 3.1. The RS2 results are compared mainly with the results from FLAC and PLAXIS. The FLAC results are obtained using the constitutive model dll file and FLAC model and FISH files from the original work by Boulanger, R. W., and Ziotopoulou, K. (<https://pm4silt.engr.ucdavis.edu/pm4silt-files>).

$s_u/\sigma'_{vc}$	$G_o$	$h_{po}$
0.25	588	20
0.50	776	50
0.75	913	60

Table 3.1. Input parameters for PM4Silt model verifications

### 3.1- Drained Monotonic Direct Simple Shear Tests

The response for drained monotonic direct simple shear tests (DSS plane-strain) for soils with  $s_u/\sigma'_{vc}$  equal to 0.25, 0.50 and 0.75 with properties listed in Table 3.1, under vertical confining stresses of 0.25, 1, 4, and 16 atmospheric pressure are presented shown in Figures 3.1 to 3.5.

All the simulations are done under strain control loading and there is a good agreement between the results generated by the three software.

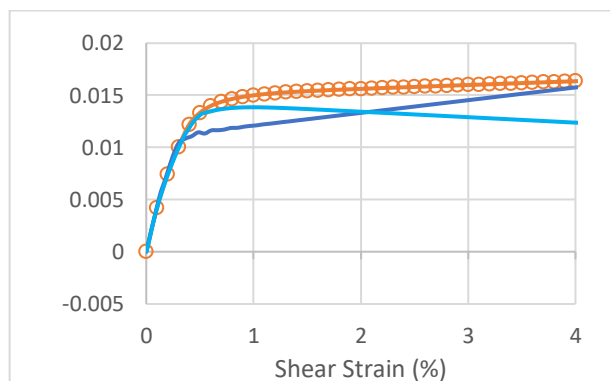
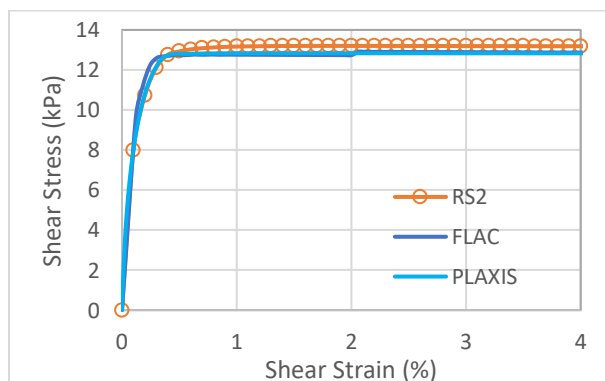
### 3.2- Undrained Monotonic Direct Simple Shear Tests

The response for undrained monotonic direct simple shear tests (DSS plane-strain) for soils with  $s_u/\sigma'_{vc}$  equal to 0.25, 0.50 and 0.75 with properties listed in Table 3.1, under vertical confining stresses of 0.25, 1, 4, and 16 atmospheric pressure are presented shown in Figures 3.6 to 3.10.

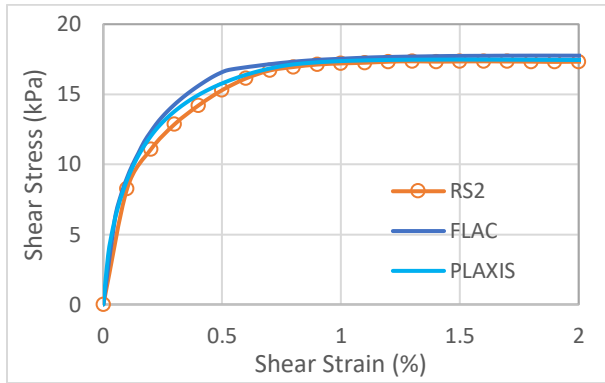
All the simulations are done under strain control loading and there is a good agreement between the results generated by the three software.

### 3.3- Undrained Cyclic Direct Simple Shear Tests

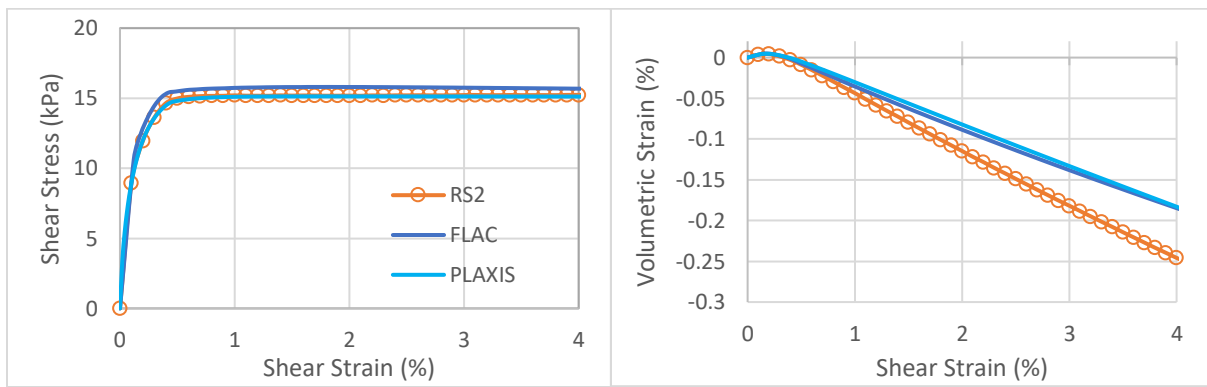
The response for undrained cyclic direct simple shear tests (DSS plane-strain) for soils with different properties as listed in Table 3.1, under vertical confining stress of 1 atmospheric pressure are presented shown in Figures 3.11 to 3.12. The simulations in FLAC are strain controlled and the loading direction changes when the shear stress reaches to the maximum/minimum values. Since the strains increments are small the maximum and minimum values of shear stress match the assigned values with an acceptable accuracy. This minor error could accumulate when the number of cycles increase, and the results might deviate form an ideal stress path with fixed minimum and maximum shear stresses. The loading in RS2 and PLAXIS is stress controlled and the accuracy of the maximum and minimum shear stresses are controlled by the tolerance defined for the convergence of the solution in these tools. Due to the difference in the loading, being strain or stress controlled, and the acceptable tolerance for the convergency of solution there are minor differences between the results, but overall, there is a good agreement between the results generated by the three software.



(a)

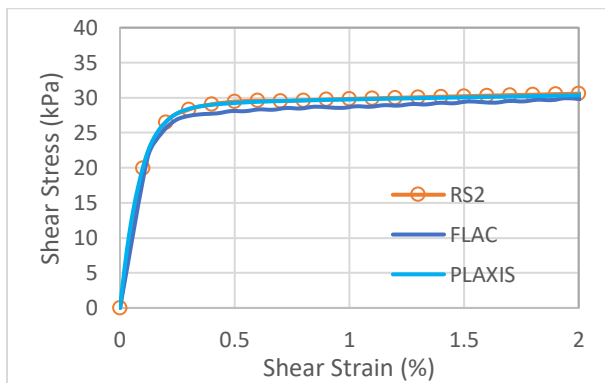


(b)

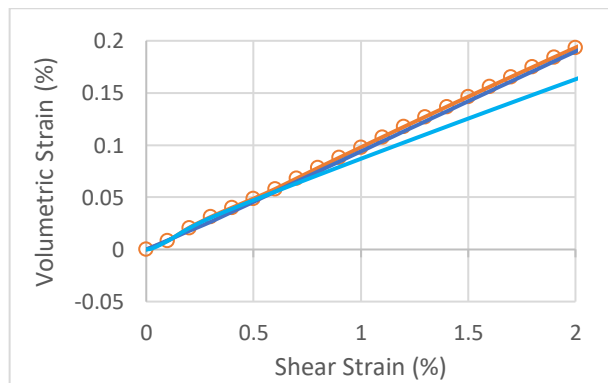


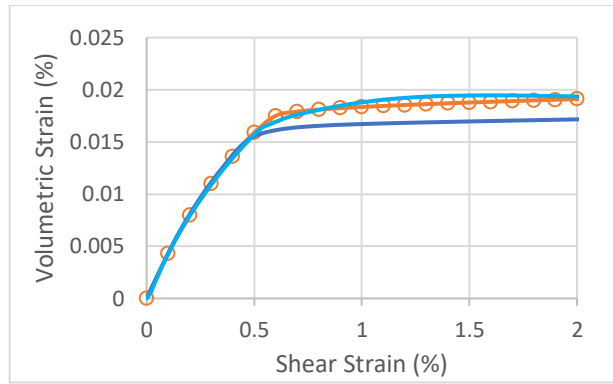
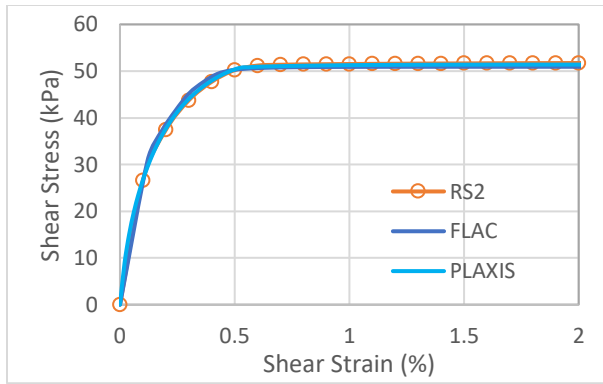
(c)

Figure 3.1. Monotonic Drained Simple Shear Test loading responses for (a)  $s_u/\sigma'_{vc} = 0.25$  (b)  $s_u/\sigma'_{vc} = 0.50$ , and (c)  $s_u/\sigma'_{vc} = 0.75$  with vertical effective stress of  $\frac{1}{4} P_{atm}$ , and  $K_o=0.5$

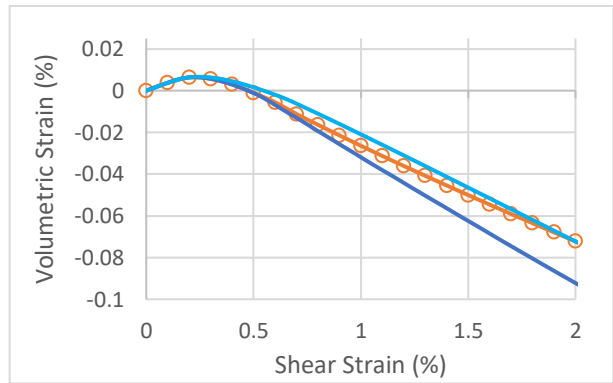
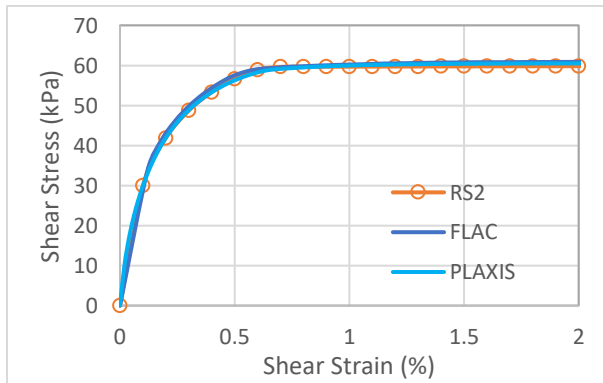


(a)



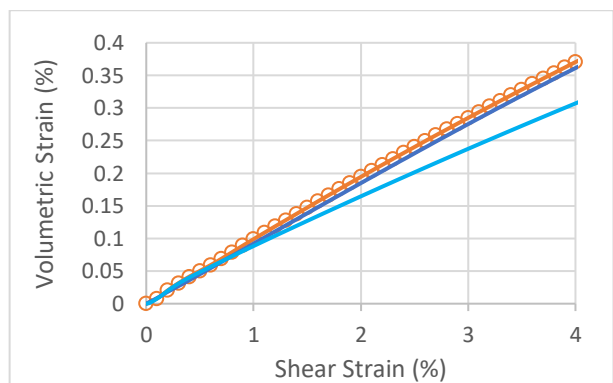
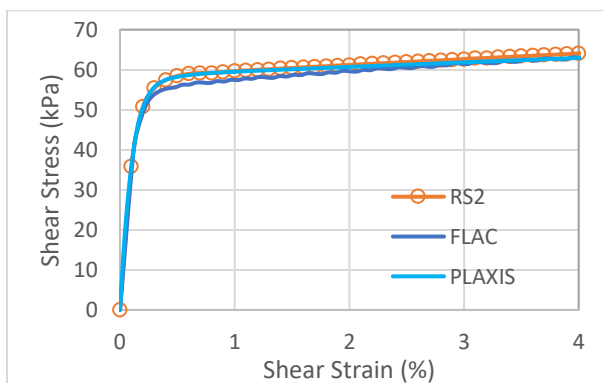


(b)

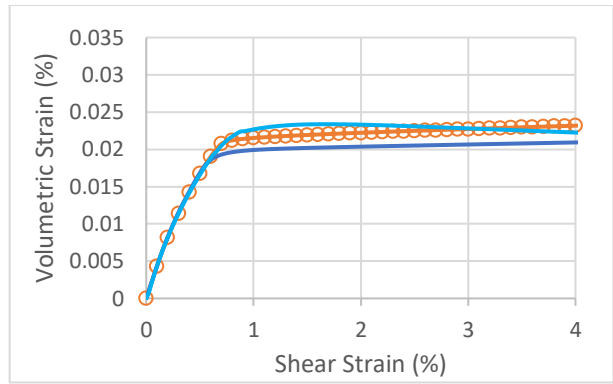
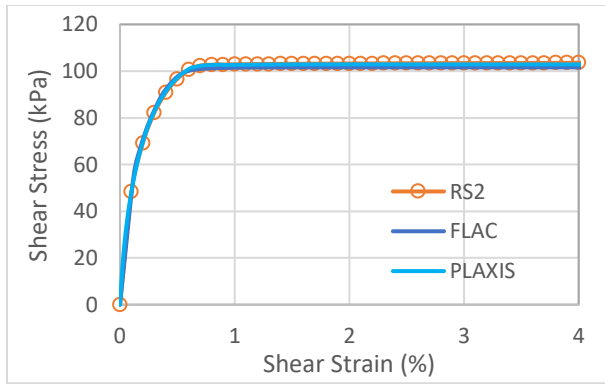


(c)

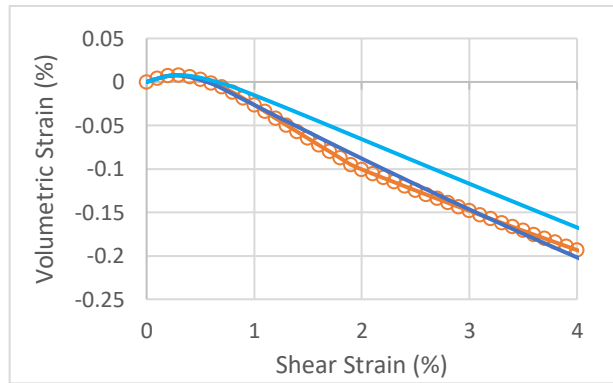
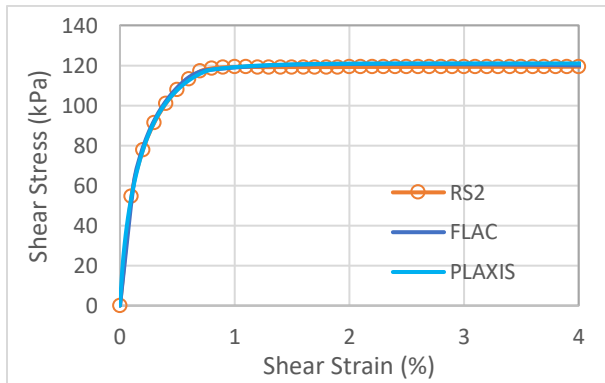
Figure 3.2. Monotonic Drained Simple Shear Test loading responses for (a)  $s_u/\sigma'_{vc} = 0.25$  (b)  $s_u/\sigma'_{vc} = 0.50$ , and (c)  $s_u/\sigma'_{vc} = 0.75$  with vertical effective stress of 1  $P_{atm}$ , and  $K_0=0.5$



(a)

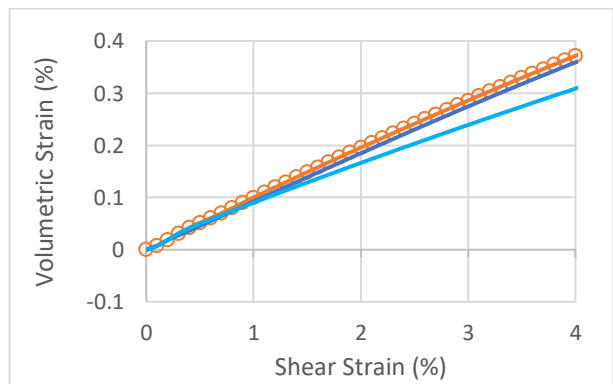
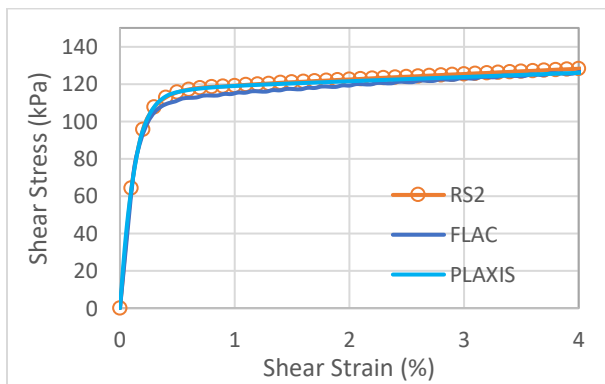


(b)



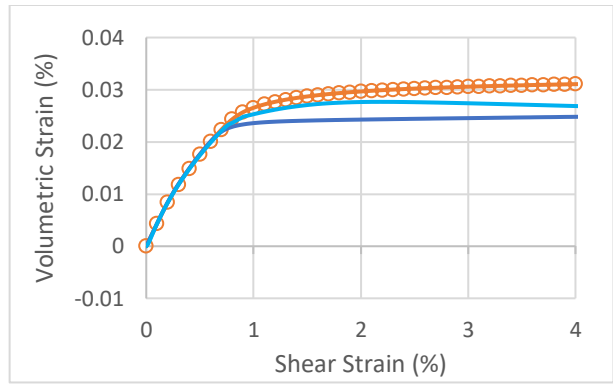
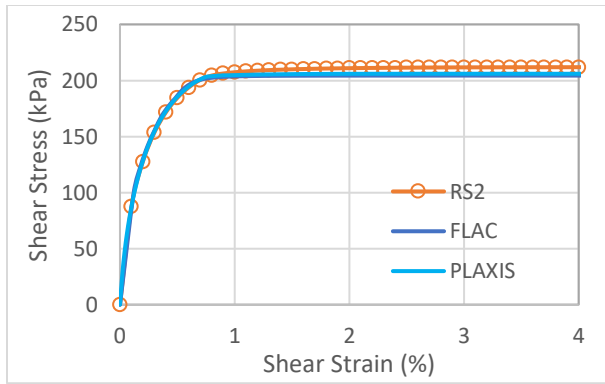
(c)

Figure 3.3. Monotonic Drained Simple Shear Test loading responses for (a)  $s_u/\sigma'_{vc} = 0.25$  (b)  $s_u/\sigma'_{vc} = 0.50$ , and (c)  $s_u/\sigma'_{vc} = 0.75$  with vertical effective stress of  $2 P_{atm}$ , and  $K_0=0.5$

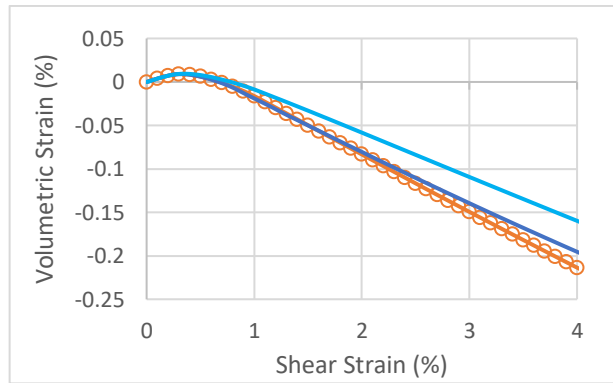
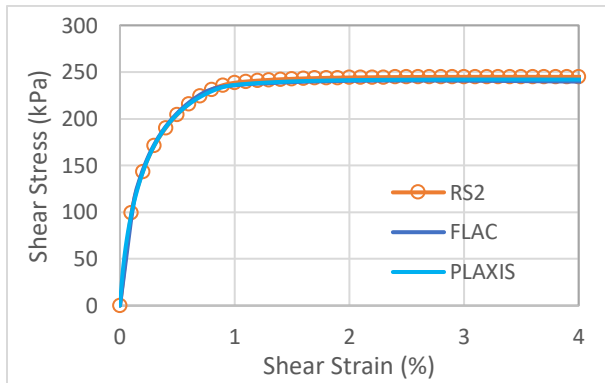


(a)



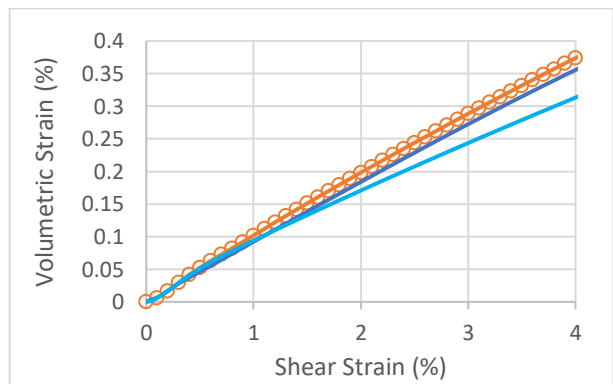
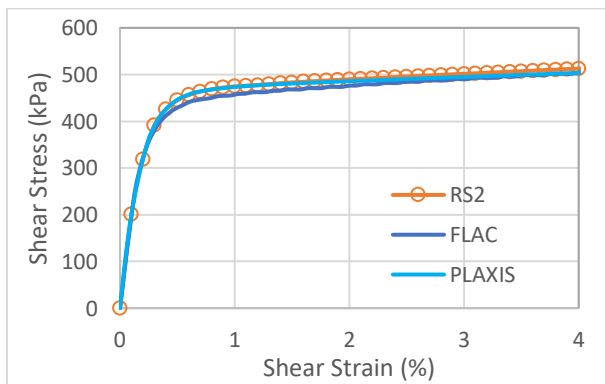


(b)

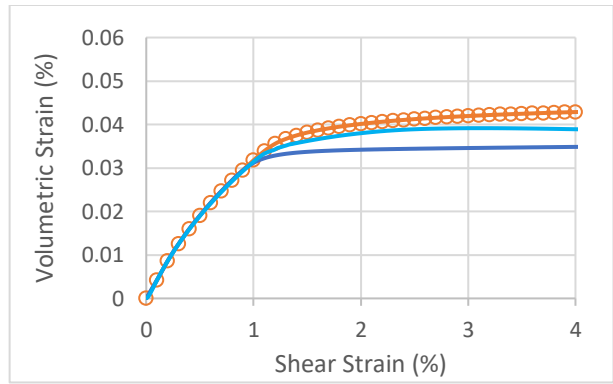
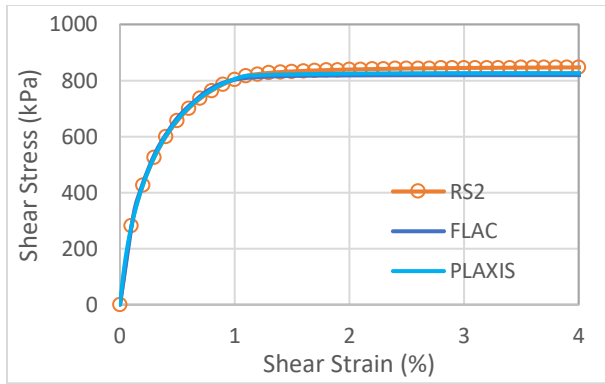


(c)

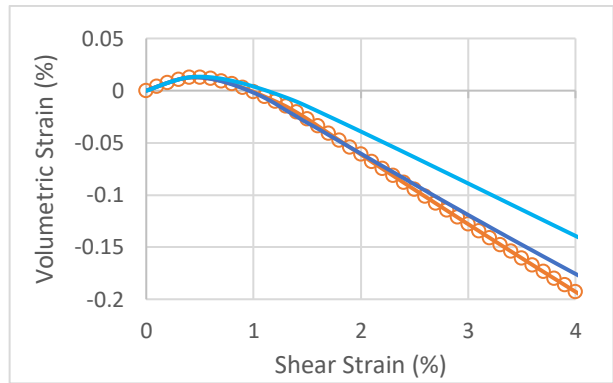
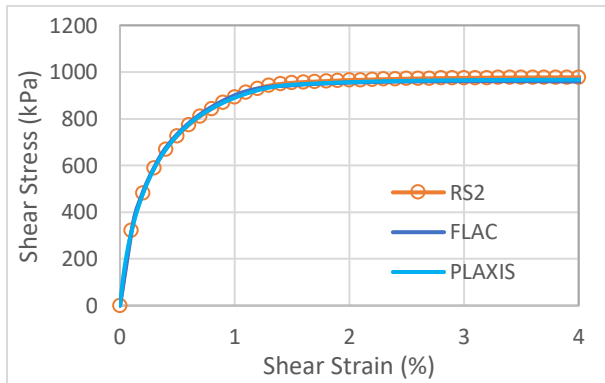
Figure 3.4. Monotonic Drained Simple Shear Test loading responses for (a)  $s_u/\sigma'_{vc} = 0.25$  (b)  $s_u/\sigma'_{vc} = 0.50$ , and (c)  $s_u/\sigma'_{vc} = 0.75$  with vertical effective stress of  $4 P_{atm}$ , and  $K_o=0.5$



(a)

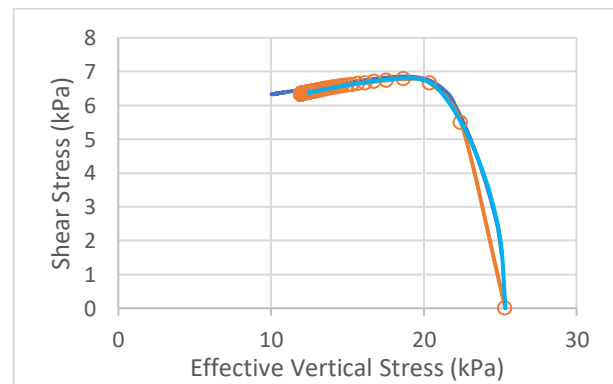
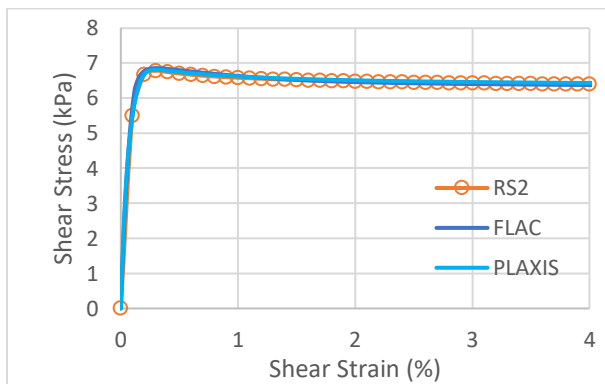


(b)

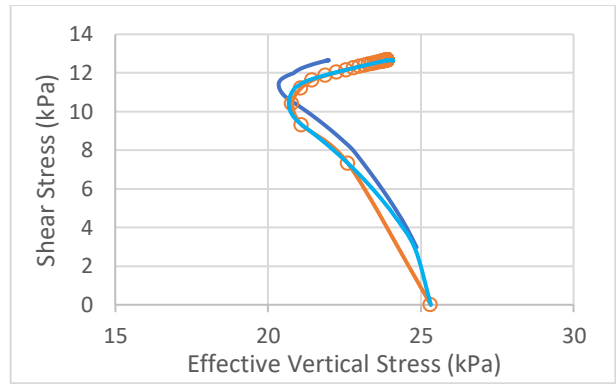
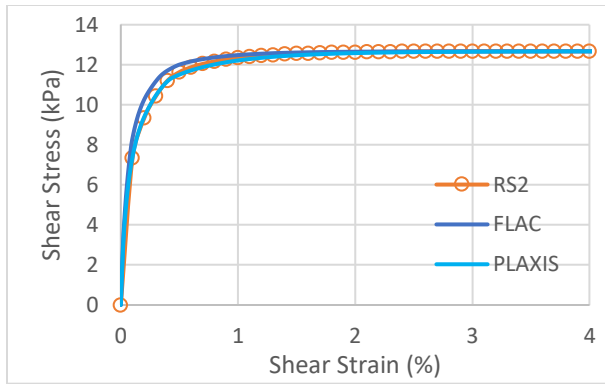


(c)

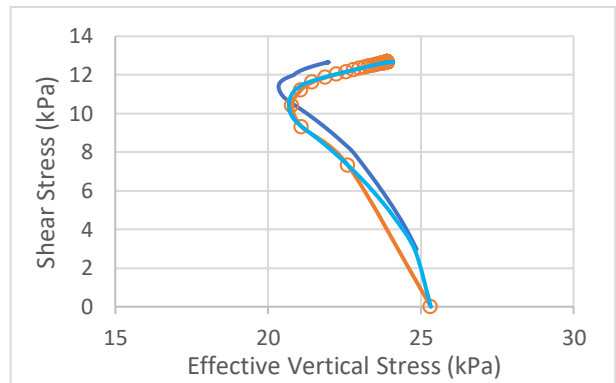
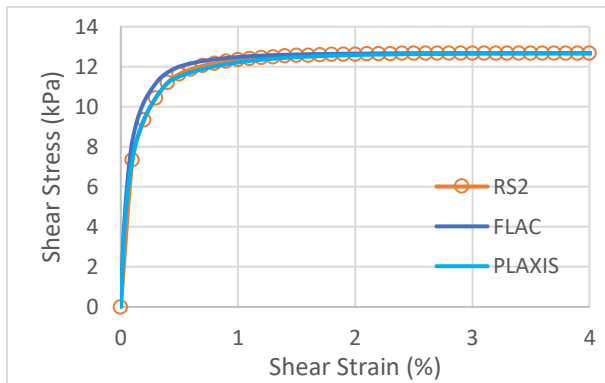
Figure 3.5. Monotonic Drained Simple Shear Test loading responses for (a)  $s_u/\sigma'_{vc} = 0.25$  (b)  $s_u/\sigma'_{vc} = 0.50$ , and (c)  $s_u/\sigma'_{vc} = 0.75$  with vertical effective stress of  $16 P_{atm}$ , and  $K_o=0.5$



(a)

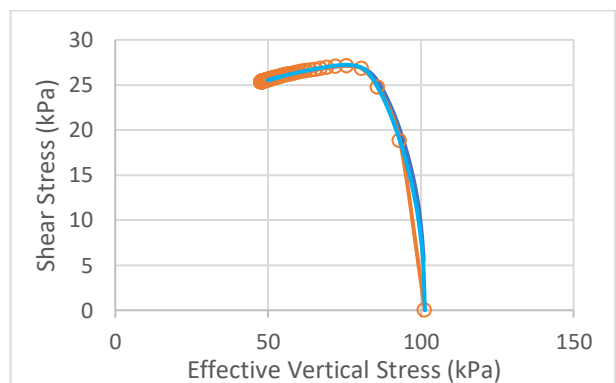
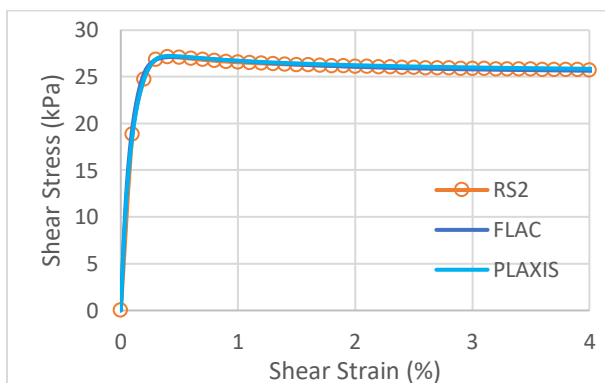


(b)

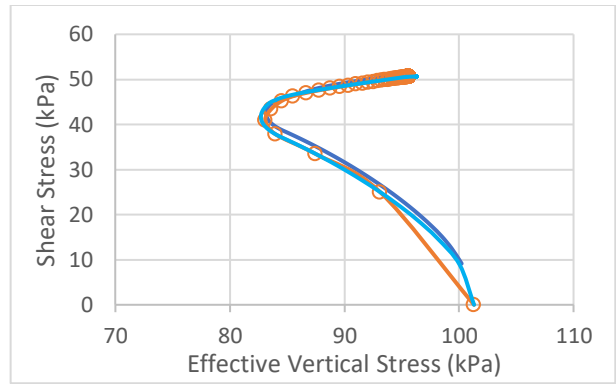
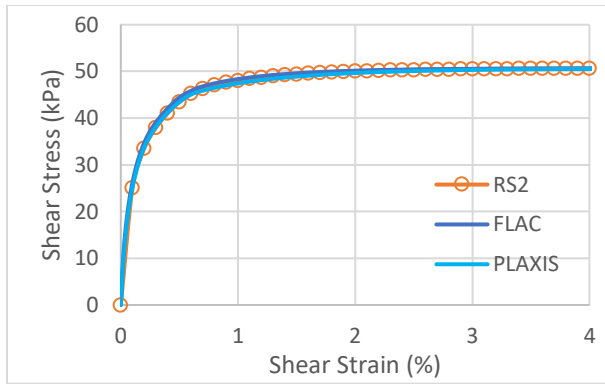


(c)

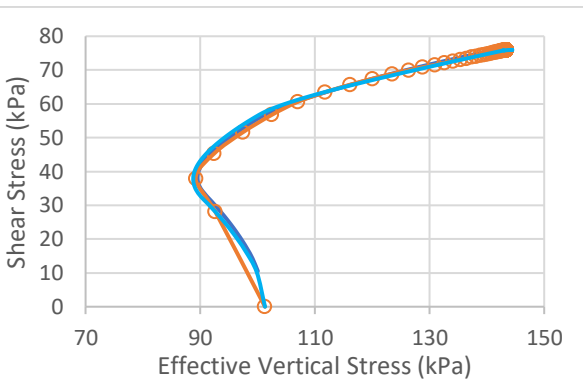
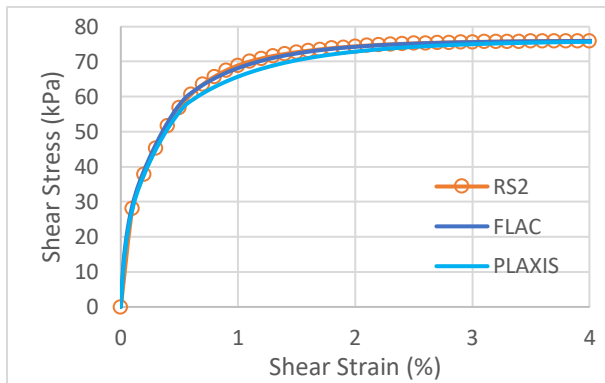
Figure 3.6. Monotonic Undrained Simple Shear Test loading responses for ((a)  $s_u/\sigma'_{vc} = 0.25$  (b)  $s_u/\sigma'_{vc} = 0.50$ , and (c)  $s_u/\sigma'_{vc} = 0.75$  with vertical effective stress of  $\frac{1}{4} P_{atm}$ , and  $K_0=0.5$



(a)

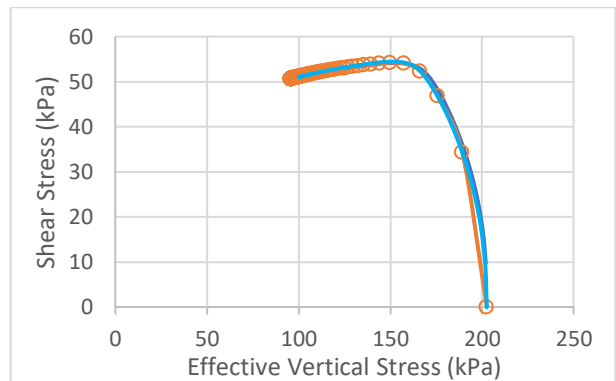
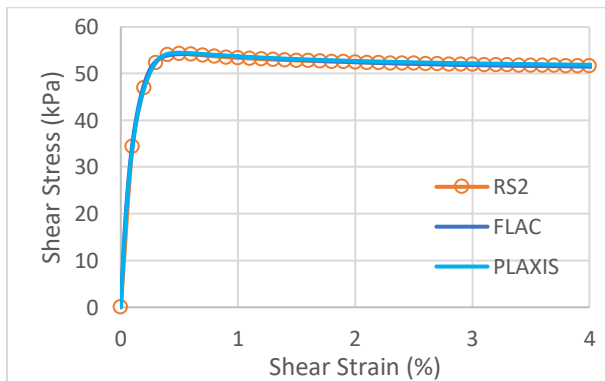


(b)

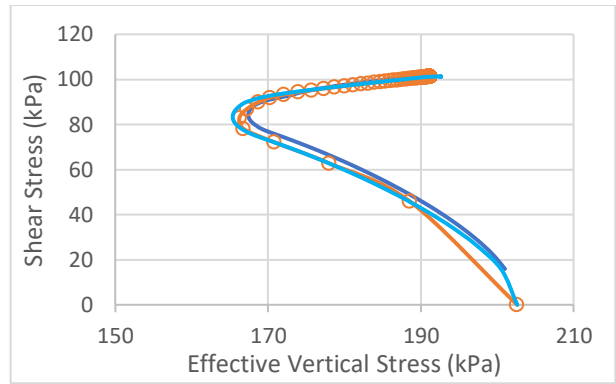
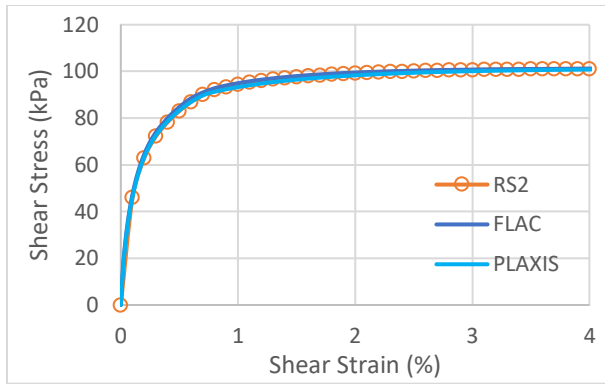


(c)

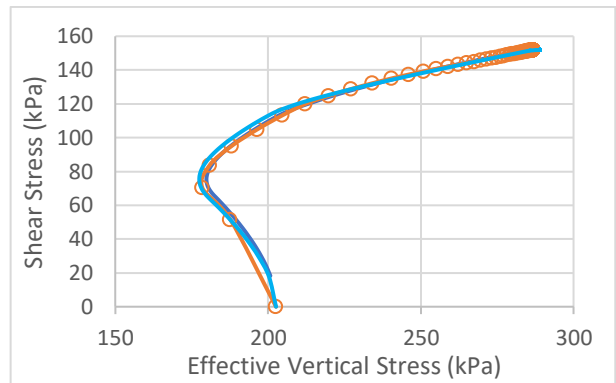
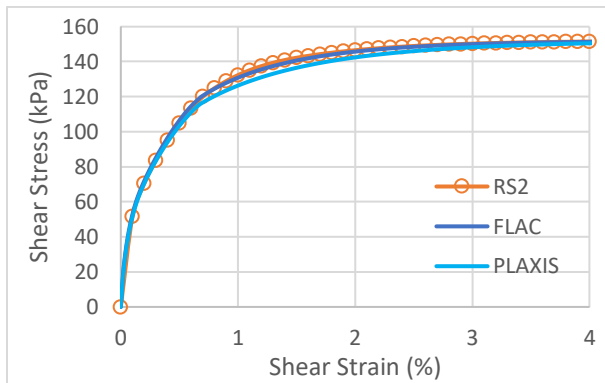
Figure 3.7. Monotonic Undrained Simple Shear Test loading responses for ((a)  $s_u/\sigma'_{vc} = 0.25$  (b)  $s_u/\sigma'_{vc} = 0.50$ , and (c)  $s_u/\sigma'_{vc} = 0.75$  with vertical effective stress of 1  $P_{atm}$ , and  $K_0=0.5$



(a)

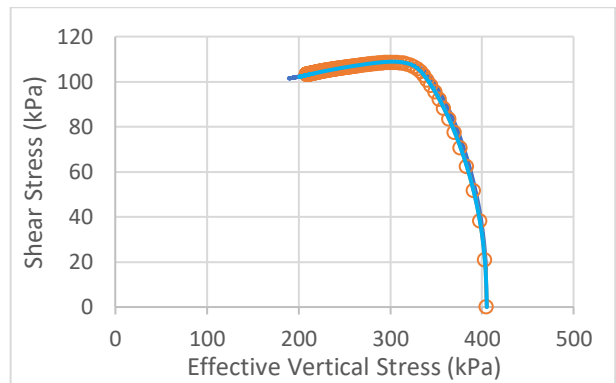
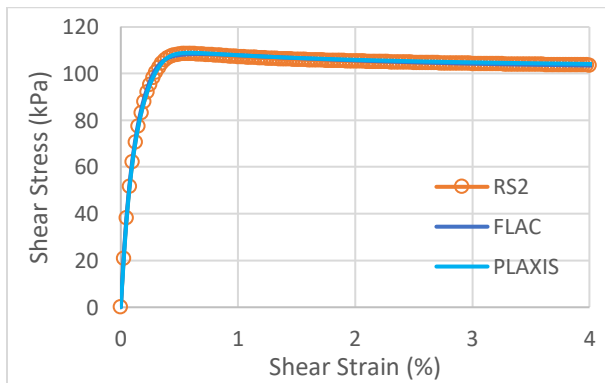


(b)

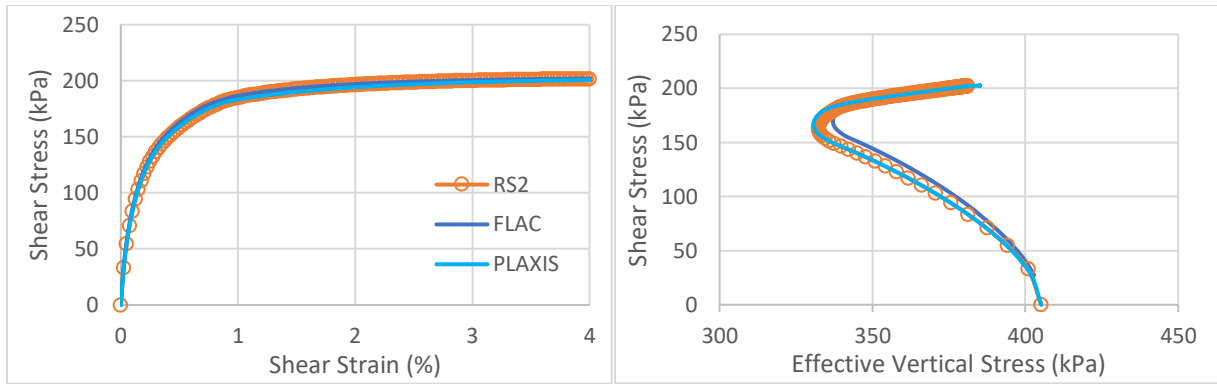


(c)

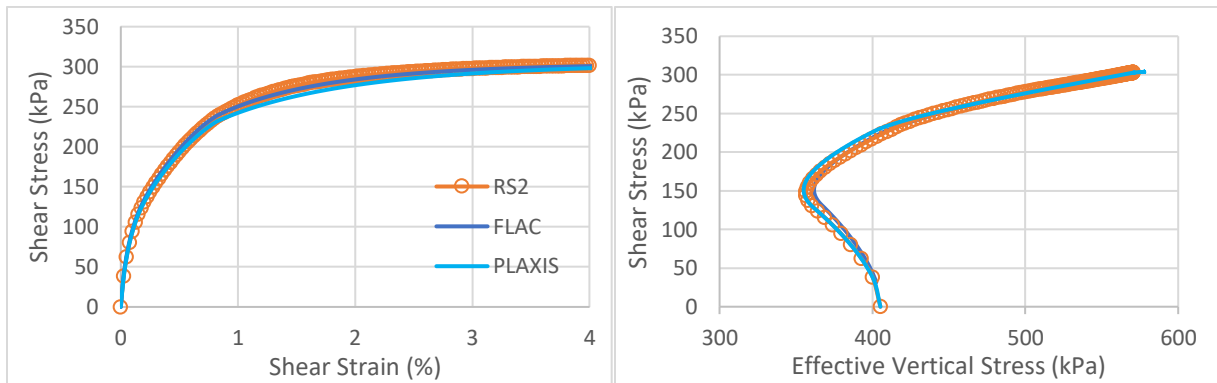
Figure 3.8. . Monotonic Undrained Simple Shear Test loading responses for ((a)  $s_u/\sigma'_{vc} = 0.25$  (b)  $s_u/\sigma'_{vc} = 0.50$ , and (c)  $s_u/\sigma'_{vc} = 0.75$  with vertical effective stress of  $2 P_{atm}$ , and  $K_0=0.5$



(a)

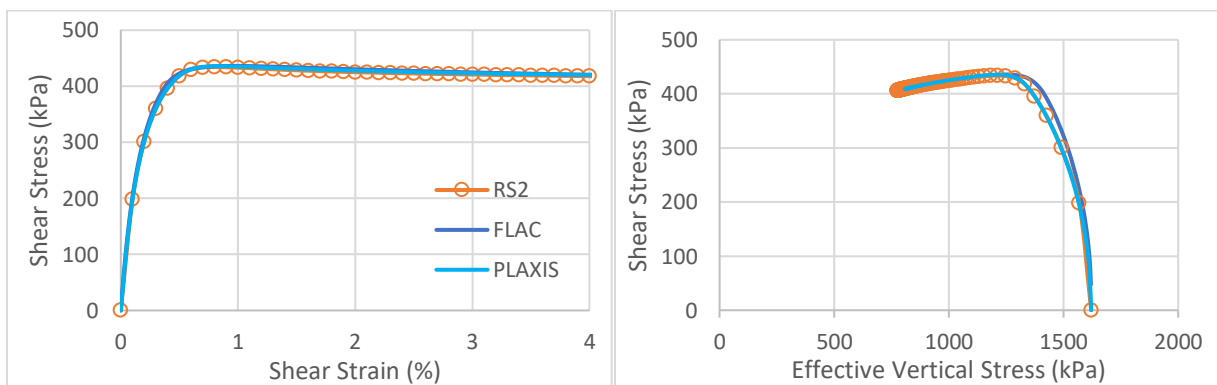


(b)

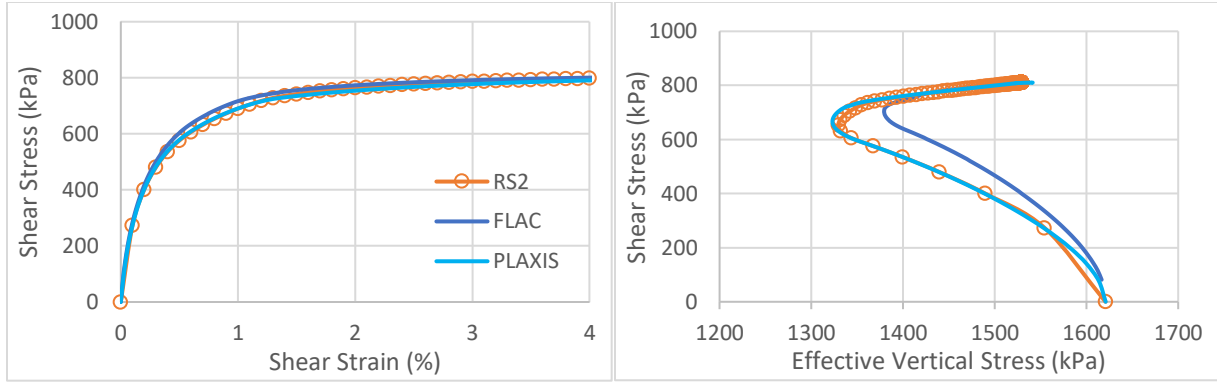


(c)

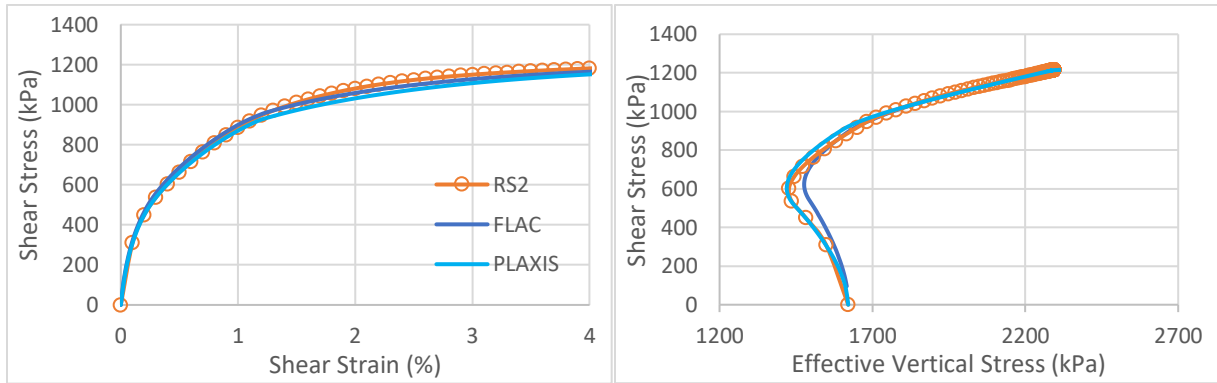
Figure 3.9. Monotonic Undrained Simple Shear Test loading responses for ((a)  $s_u/\sigma'_{vc} = 0.25$  (b)  $s_u/\sigma'_{vc} = 0.50$ , and (c)  $s_u/\sigma'_{vc} = 0.75$  with vertical effective stress of  $4 P_{atm}$ , and  $K_0=0.5$



(a)



(b)



(c)

Figure 3.10. Monotonic Undrained Simple Shear Test loading responses for ((a)  $s_u/\sigma'_{vc} = 0.25$  (b)  $s_u/\sigma'_{vc} = 0.50$ , and (c)  $s_u/\sigma'_{vc} = 0.75$  with vertical effective stress of  $16 P_{atm}$ , and  $K_o=0.5$

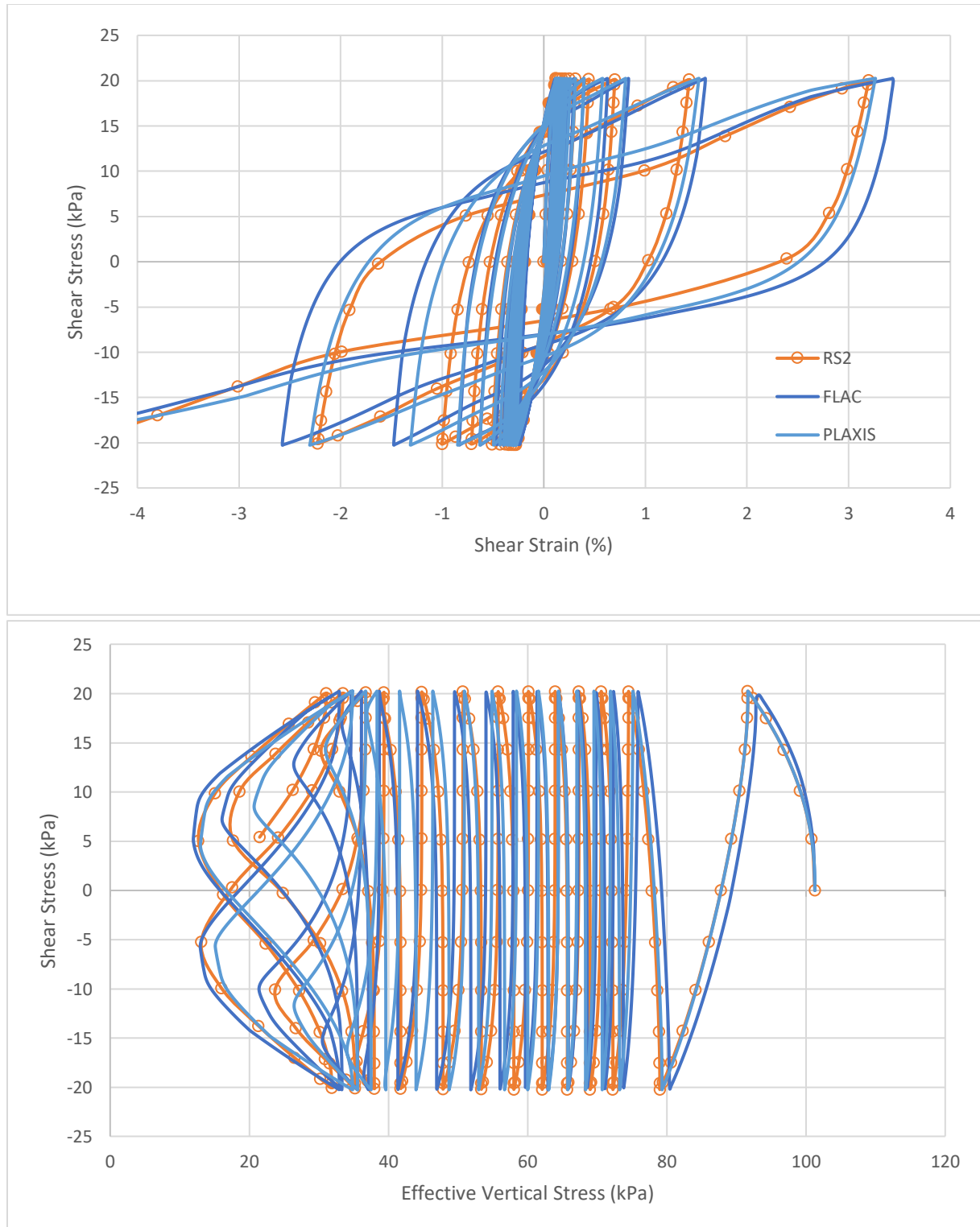


Figure 3.11. Cyclic Undrained Simple Shear Test loading responses for  $s_u/\sigma'_{vc} = 0.25$  under vertical effective stress of  $1 P_{atm}$ , and  $K_0=0.5$  with maximum loading ratio of  $\tau/P_{atm} = 0.2$ ; (a) variation of share stress with shear strain and (b) effective stress path



## References

Been, K., and Jefferies, M. G. (1985). "A state parameter for sands." *Géotechnique* 35(2), 99–112.

Boulanger, R. W., & Ziotopoulou, K. (2017). PM4Sand (version 3.1): A sand plasticity model for earthquake engineering applications. Rep. No. UCD/CGM-17/01. Davis, CA: Center for Geotechnical Modeling, Dept. of Civil and Environmental Engineering, Univ. of California.

Boulanger, R. W. and Ziotopoulou, K. (2018). "PM4SILT (Version 1): a silt plasticity model for earthquake engineering applications." Report No. UCD/CGM-18/01, Center for Geotechnical Modeling, University of California at Davis.

Dafalias, Y. F., and Manzari, M. T. (2004). "Simple plasticity sand model accounting for fabric change effects." *Journal of Engineering Mechanics*, ASCE, 130(6), 622-634.

Itasca (2016). FLAC – Fast Lagrangian Analysis of Continua, Version 8.0, Itasca Consulting Group, Inc., Minneapolis, Minnesota.

Plaxis, "User's manual of PLAXIS." (2018).

Ziotopoulou, K., and Boulanger, R. W. (2012). "Constitutive modeling of duration and overburden effects in liquefaction evaluations." 2nd International Conference on Performance-Based Design in Earthquake Geotechnical Engineering, ISSMGE, Taormina, Italy, May 28-30, paper no. 03.10, 467-482.